

DOUBLE NEUTRON STAR MERGERS FROM HIERARCHICAL TRIPLE-STAR SYSTEMS

ADRIAN S. HAMERS¹ AND TODD A. THOMPSON^{2,3,1}

¹Institute for Advanced Study, School of Natural Sciences, Einstein Drive, Princeton, NJ 08540, USA

²Department of Astronomy, The Ohio State University, Columbus, Ohio 43210, USA

³Center for Cosmology and AstroParticle Physics, Department of Physics, The Ohio State University, Columbus, Ohio 43210, USA

Draft version August 13, 2019

Abstract

The isolated binary evolution model for merging neutron stars (NSs) involves processes such as mass transfer, common-envelope evolution, and natal kicks, all of which are poorly understood. Also, the predicted NS-NS merger rates are typically lower than the rates inferred from the LIGO GW170817 event. Here, we investigate merger rates of NS and black hole (BH)-NS binaries in hierarchical triple-star systems. In such systems, the tertiary can induce Lidov-Kozai (LK) oscillations in the inner binary, accelerating its coalescence, and potentially enhancing compact object merger rates. However, since compact objects originate from massive stars, the prior evolution should also be taken into account. Natal kicks, in particular, could significantly reduce the rates by unbinding the tertiary before it can affect the inner binary through LK evolution. We carry out simulations of massive triples taking into account stellar evolution starting from the main sequence, secular and tidal evolution, and the effects of supernovae. For large NS birth kicks ($\sigma_k = 265 \text{ km s}^{-1}$), we find that the triple NS-NS merger rate (several hundred $\text{Gpc}^{-3} \text{ yr}^{-1}$) is lower by a factor of $\sim 2 - 3$ than the binary rate, but for no kicks ($\sigma_k = 0 \text{ km s}^{-1}$), the triple rate (several thousand $\text{Gpc}^{-3} \text{ yr}^{-1}$) is comparable to the binary rate. Our results indicate that a significant fraction of NS-NS mergers could originate from triples if a substantial portion of the NS population is born with low kick velocities, as indicated by other work. However, uncertainties and open questions remain because of our simplifying assumption of dynamical decoupling after inner binary interaction has been triggered.

Keywords: binaries: general – stars: neutron – stars: kinematics and dynamics – stars: evolution – gravitation

1. INTRODUCTION

The detection of a double neutron star (NS) merger by LIGO’s O2 observing run (Abbott et al. 2017b) has definitively shown that double neutron stars (NSs) can merge in the Universe, and the accompanying electromagnetic signals in gamma rays (e.g., Abbott et al. 2017a; Goldstein et al. 2017; Savchenko et al. 2017), X-rays (e.g., Margutti et al. 2017), optical (e.g., Coulter et al. 2017; Shappee et al. 2017; Soares-Santos et al. 2017; Nicholl et al. 2017), near-infrared (e.g., Chornock et al. 2017; Cowperthwaite et al. 2017; Pian et al. 2017), and radio wavelengths (e.g., Alexander et al. 2017), have revealed a wealth of information on kilonova transients (e.g., Lattimer & Schramm 1974; Freiburghaus et al. 1999; Metzger et al. 2010; Rosswog 2015; Just et al. 2015), and short gamma-ray bursts (e.g., Eichler et al. 1989; Piran 1999; Berger 2014). The origin of compact object mergers is unclear, since in standard stellar evolution theory, the progenitor stars would merge before evolving to compact objects in an orbit that would cause them to merge due to gravitational wave (GW) emission within a Hubble time. Two main scenarios have been proposed for compact object mergers: isolated binary evolution (e.g., Tutukov & Yungelson 1973; Tutukov et al. 1992; Tutukov & Yungelson 1993; Lipunov et al. 1997; Belczynski et al. 2002; Voss & Tauris 2003; Kalogera et al. 2007; Dominik et al. 2012, 2013; Belczynski et al. 2014, 2016a, 2017; Stevenson et al. 2017; Chruslinska et al. 2018; Giacobbo & Mapelli 2019) and dynamical interactions, such as those in triple-star systems (e.g., Thompson 2011; Hamers et al. 2013; Antonini et al. 2017; Silsbee & Tremaine 2017; Liu & Lai 2017, 2018; Toonen et al. 2018; Liu et al. 2019), globular clusters (e.g., Sigurdsson & Hernquist 1993; Porte-

gies Zwart & McMillan 2000; O’Leary et al. 2006; Ziosi et al. 2014; Rodriguez et al. 2015, 2016; Kimpson et al. 2016; Mapelli 2016; Samsing & Ramirez-Ruiz 2017; Samsing et al. 2018a,b; Samsing 2018; Rodriguez et al. 2018), and galactic nuclei (e.g., Antonini & Perets 2012; Antonini et al. 2014; Prodan et al. 2015; Stephan et al. 2016; VanLandingham et al. 2016; Antonini & Rasio 2016; Petrovich & Antonini 2017; Arca-Sedda & Gualandris 2018; Randall & Xianyu 2018a,b; Hamers et al. 2018; Gondán et al. 2018; Hoang et al. 2018; Fragione et al. 2018; Arca-Sedda & Capuzzo-Dolcetta 2019).

The isolated binary channel involves binary interactions such as mass transfer, common-envelope (CE) evolution, and supernovae (SNe) kicks associated with the birth of NSs or black holes (BHs). The details of these processes are highly uncertain, yet, taking into account these uncertainties, it is challenging in the isolated binary model to predict rates (e.g., Kalogera et al. 2004b,a, see also Abadie et al. 2010 for a review) that are on the same order of magnitude as derived from the LIGO observation of GW170817, $1540^{+3200}_{-1220} \text{ Gpc}^{-3} \text{ yr}^{-1}$ (Abbott et al. 2017b). For example, Giacobbo & Mapelli (2018) find rates of up to $1 \times 10^3 \text{ Gpc}^{-3} \text{ yr}^{-1}$, but only assuming low SNe kicks, and a high CE efficiency.

Triple systems have been invoked in a large variety of contexts to explain an enhanced rate of interaction in binary systems (see, e.g., Naoz 2016 for a review). This occurs through oscillations of the inner binary eccentricity as a result of the torque of the tertiary, known as Lidov-Kozai (LK) oscillations (Lidov 1962; Kozai 1962). In particular, in the context of compact objects, it has been suggested that LK-driven eccentricity excitation can accelerate the mergers of compact objects (e.g., Blaes et al. 2002; Miller & Hamilton 2002; Wen 2003; Thompson 2011; Antonini et al. 2017; Hoang et al. 2018; Bonetti et al. 2018; Stephan et al. 2019; Fragione &

Loeb 2019). However, since compact objects originate from massive stars¹, the prior stellar evolution should also be taken into account, similarly to studies of binary evolution (e.g., Hamers et al. 2013; Stephan et al. 2016; Naoz et al. 2016; Toonen et al. 2018; Hamers 2018a; Stephan et al. 2019). Natal kicks, in particular, could significantly reduce the rates by unbinding the tertiary before it can affect the inner binary through LK evolution (e.g., Lu & Naoz 2019; Hamers & Thompson 2019).

In this paper, we investigate the interplay between these processes in massive triple-star systems, taking into account stellar evolution starting from the main sequence (MS), secular and tidal evolution, and the effects SNe. In contrast to previous studies which focused on wide inner binaries that do not interact in the absence of a tertiary star (e.g., Hamers et al. 2013; Antonini et al. 2017; Hamers & Thompson 2019), we here consider triples with no restrictions on the inner binary orbital separation. In particular, this implies that in the ‘binary case’ of our triples, i.e., when the effect of the tertiary on the inner binary is ignored, the system can in fact interact, and possibly produce a double NS merger via the standard binary evolution channel.

This approach requires to model binary processes such as mass transfer and CE evolution, as well as the effects associated with the gravitational perturbations from the tertiary (i.e., LK oscillations). Combining these processes is challenging and complicated (see, e.g., Hamers & Dosopoulou 2019 for an exploratory study for the case of mass transfer taking into account orbital effects due to mass transfer and LK evolution). Here, we take a simpler approach in which we model the evolution of the tertiary initially using a secular code taking into account dynamical, stellar and tidal evolution, but not mass transfer nor CE evolution. We track the onset of mass transfer (i.e., Roche-Lobe overflow, RLOF), and in this case, we continue the evolution of the inner binary system using a dedicated binary population synthesis code which includes all the required binary physics, but not any effects associated with the tertiary star. Here, we make the assumption that, after the onset of RLOF in the inner binary, the latter is dynamically decoupled from the tertiary. This assumption is typically justified in the case of CE evolution, in which case the inner binary shrinks significantly (see Fig. 8 of Hamers et al. 2013). However, in the case of mass transfer, the inner orbit can also expand (if the donor has become less massive than the accretor). We here ignore this complication, but instead take the simpler, decoupled approach.

Several types of compact object mergers have been studied in triple systems, including WD-WD mergers (Thompson 2011; Katz & Dong 2012; Hamers et al. 2013; Toonen et al. 2018; Stephan et al. 2019), BH-BH mergers (Silsbee & Tremaine 2017; Antonini et al. 2017; Liu & Lai 2017, 2018; Hoang et al. 2018; Liu et al. 2019), and BH-NS mergers (Stephan et al. 2019; Fragione & Loeb 2019). To our knowledge, NS-NS mergers in triples with stellar-mass tertiaries (taking into account stellar evolution and dynamical evolution; see Stephan et al. 2019 for a comparable study, but with supermassive BH tertiaries) have not been studied. Our focus is therefore on mergers of double NSs.

The structure of this paper is as follows. We describe our methodology in Section 2, and the initial conditions of our simulations in Section 3. We present our results, most notably the merger rates, in Section 4. We discuss our findings in

Section 5, and conclude in Section 6.

2. NUMERICAL METHOD

We use a hybrid method in which we use SECULARMULTIPLE (Hamers & Portegies Zwart 2016a; Hamers 2018b) to model the secular dynamical, tidal, and stellar evolution of a binary or hierarchical triple star system, and the binary stellar evolution code BSE (Hurley et al. 2000, 2002) to model the evolution of systems in which we consider the tertiary to be unimportant. The latter case, which we will refer to as ‘isolated’ binary evolution, includes interacting systems that undergo mass transfer in the inner binary, and systems in which the tertiary star becomes unbound from the inner binary due to a SNe event but with the inner binary remaining bound, and possibly merging at a later time. Both codes, SECULARMULTIPLE and BSE, are implemented within the AMUSE framework (Portegies Zwart et al. 2013; Pelupessy et al. 2013).

2.1. SECULARMULTIPLE

In SECULARMULTIPLE, we model the evolution of a binary or triple system, starting from MS stars, and taking into account stellar evolution, tidal evolution, and secular dynamical evolution (in the case of triples, and up to and including fifth order in the expansion of the separation ratio of the inner to the outer binary, see Hamers & Portegies Zwart 2016a; Hamers 2018b²). The modeling in SECULARMULTIPLE is similar to that in previous works in which we coupled secular dynamical evolution to stellar and tidal evolution (Hamers & Portegies Zwart 2016b; Hamers 2018a; Hamers & Thompson 2019).

Stellar evolution is taken into account by using SSE (Hurley et al. 2000) (as implemented in AMUSE), which is based on analytical fits to detailed stellar evolution models, and which uses the same stellar tracks as (i.e., is consistent with) BSE. We set the metallicity to Solar, $Z = 0.02$. Quantities that are used from SSE include the stellar type and (convective envelope) mass and radius as a function of age. These quantities are used to take into account mass loss from the system, assumed to occur either adiabatically, or because of an impulsive change due to SNe. In the former case, we assume isotropic and adiabatic mass loss, i.e., $a_i M_i$ and e_i are constant (Huang 1956, 1963) for an orbit i in the system ($i = 1$ and $i = 2$, for the inner and outer orbits, respectively, and if applicable). Here, $M_1 = m_1 + m_2$ for the inner orbit, and $M_2 = M_1 + m_3$ for the outer orbit.

In the case of SNe, we use the routines incorporated into SECULARMULTIPLE and described in Hamers (2018b) to compute the effects on the inner and outer orbits of the (assumed to be instantaneous) mass loss and (possible) kick to the newly-formed NS or BH, assuming a random orbital phase of both orbits at the moment of SNe. We assume that the kick distribution is a Maxwellian distribution, i.e., the probability density function of the kick speed V_k is given by

$$\frac{dN}{dV_k} = \sqrt{\frac{2}{\pi}} \frac{V_k^2}{\sigma_k^3} \exp\left(-\frac{V_k^2}{2\sigma_k^2}\right). \quad (1)$$

Here, σ_k characterizes the typical kick speed, and is assumed to be given (see Section 3 below). For BHs, we use the prescription of Fryer et al. (2012, Section 4.1) to rescale the sampled speed V_k in equation (1) according to $V_{k,BH} = V_k(1 - f_{fb})$,

¹ Excluding the possibility of primordial compact objects.

² The reference frame in SECULARMULTIPLE is an arbitrary frame, rather than the invariable plane.

where the fallback factor f_{fb} is given by

$$f_{\text{fb}} = \begin{cases} 0, & M_{\text{CO}} < 5 M_{\odot}; \\ 0.378 M_{\text{CO}} - 1.889, & 5.0 M_{\odot} \leq M_{\text{CO}} < 7.6 M_{\odot}; \\ 1, & M_{\text{CO}} \geq 7.6 M_{\odot}. \end{cases} \quad (2)$$

where M_{CO} is the mass of the carbon-oxygen core of the proto-BH, which is extracted from SSE.

Tidal evolution is taken into account with the assumption of the equilibrium tide model (Hut 1981; Eggleton et al. 1998). Specifically, we use equations (81) and (82) of Eggleton et al. (1998), with the non-dissipative terms X , Y and Z given explicitly by equation (10)-(12) of Eggleton & Kiseleva-Eggleton (2001), and the dissipative terms V given explicitly by equations (A7)-(A11) of Barker & Ogilvie (2009). We apply these terms to both the inner and outer orbits (if applicable), in the latter case treating the inner binary as a point mass. The stellar spins are included in the tidal calculations; the initial spin-orbit angles are assumed to be zero (i.e., zero obliquities). The tidal dissipation efficiency is computed as a function of the stellar parameters as part of the set of ordinary differential equations using the prescription of Hurley et al. (2002). For all stars, we assume a fixed apsidal motion constant of $k_{\text{AM},i} = 0.014$, and a gyration radius of 0.08 (these parameters are not provided by SSE in AMUSE).

Many uncertainties still remain in tidal evolution (see, e.g., Ogilvie 2014 for a review). Especially for high eccentricities, which could be excited by LK oscillations, the equilibrium tide model could break down. A more sophisticated treatment of tides is beyond the scope of this work.

During the integration of the system in SECULARMULTIPLE, we check for a number of stopping conditions. These are listed and explained below.

1. For both binaries and triples, we check for RLOF in the inner binary using analytic fits (Sepinsky et al. 2007, eqs. 47-52). Specifically, we check for RLOF at periastris as a function of the current radii, spins, and inner binary semimajor axis and eccentricity. If RLOF occurs, we stop the simulation within SECULARMULTIPLE, and continue the evolution of the inner binary using BSE; see Section 2.2 below for further details. We also check for RLOF by the tertiary star on the inner binary, treating the binary as a point mass and using the same fits of Sepinsky et al. (2007), although this scenario occurs much less commonly compared to RLOF in the inner binary (see Tables 2 and 3).
2. For both binaries and triples, after each SNe event, we check if the system is still bound (i.e., if $a_i > 0$ for $i = 1$ and $i = 2$ if applicable). If not, we continue the evolution of the inner binary with BSE if the outer orbit became unbound, but the inner binary is still bound (and could interact and merge at a later time); see Section 2.2 below.
3. For triples, we check for dynamical stability of the system using the criterion of Mardling & Aarseth (2001), and stop the simulation in SECULARMULTIPLE if the system is unstable according to this criterion. We do not consider the subsequent evolution of the system.
4. For triples, we check if at any point in the evolution if the secular approximation made in the equations of motion breaks down. Such a breakdown can occur if the timescale for the inner binary angular momentum

to change significantly becomes comparable to the inner or outer orbital periods (e.g., Čuk & Burns 2004; Ivanov et al. 2005; Katz & Dong 2012; Antonini & Perets 2012; Seto 2013; Antonini et al. 2014; Antognini et al. 2014; Bode & Wegg 2014; Luo et al. 2016; Lei et al. 2018; Grishin et al. 2018). To evaluate whether or not this has occurred, we use the criterion of Antonini et al. (2014), i.e.,

$$\sqrt{1 - e_1} < 5\pi \frac{m_3}{m_1 + m_2} \left[\frac{a_1}{a_2(1 - e_2)} \right]^3. \quad (3)$$

Although we check for this regime (also known as the semisecular regime), it occurs very rarely in our simulations since extremely high eccentricities are required, and in most cases this implies that the stars in the inner binary would undergo mass transfer well before.

5. The inner binary components collide directly, i.e., $a_1(1 - e_1) < R_1 + R_2$, where R_1 and R_2 are the primary and secondary radius, respectively. This typically can only occur for compact objects, since the larger sizes of pre-compact objects generally imply that, when the eccentricity is high, usually RLOF occurs or possibly the semisecular regime is triggered.
6. The system exceeds an age of 10 Gyr.

In contrast to previous work related to white dwarfs (Hamers 2018a; Hamers & Thompson 2019), we here do not include the effects of flybys on the binary or triple system. We find that most NS-NS mergers occur relatively early, i.e., within ~ 100 Myr (see Section 4 below). For systems in the field, flybys are typically unimportant on such time-scales. Mergers occurring as a result of perturbations from passing stars are beyond the scope of this paper (see, e.g., Kaib & Raymond 2014; Michaely & Perets 2019).

2.2. BSE

As described in Section 2, we consider two situations in the simulations with SECULARMULTIPLE in which we assume for triples that the inner binary can subsequently be decoupled from the tertiary star. We then continue the evolution with the binary population synthesis code BSE. The latter code includes prescriptions for binary-star evolution, most notably mass transfer and CE evolution, which are both not modeled in SECULARMULTIPLE. In BSE, we assume a CE binding energy factor of $\lambda = 0.5$, and a CE efficiency of $\alpha = 1$. Furthermore, in BSE we assume the same NS kick speed distribution as in SECULARMULTIPLE (see equation 1). Due to limitations of BSE, we do not include the fallback correction to kicks applied to BHs, as described by equation (2). Instead, in BSE, we assume zero kick speeds for BHs. This is strictly inconsistent with the prior simulations in SECULARMULTIPLE, but our main focus in this work is on merging NSs, so we do not expect this inconsistency to strongly affect our conclusions.

The two situations in which we hand off the evolution in SECULARMULTIPLE to BSE correspond to stopping conditions (1) and (2) described in Section 2.1. In situation (1), the inner binary undergoes RLOF, which can be triggered by several factors: expansion of the stars in the inner binary due to stellar evolution, possibly combined with tidal evolution, and/or high eccentricity due to secular evolution. Note that, contrary

to previous studies, we do not restrict to wide systems. Therefore, many systems will undergo RLOF even in the ‘binary’ case, i.e., in absence of a tertiary star.

The crucial assumption made in situation (1) for triples is that the subsequent evolution of the inner binary is completely decoupled from the tertiary star. This is a strong assumption, and is certainly not correct for all systems. The motivation for this approach is simplicity, since we currently do not have the tools to self-consistently simulate the evolution of the triple system taking into account the secular dynamical evolution with mass transfer, in particular if the orbit is eccentric and driven to varying eccentricity due to LK oscillations with similar RLOF and LK time-scales. Preliminary work (Hamers & Dosopoulou 2019) indicates that the evolution in this regime is complicated, and merits future study. The decoupling assumption likely gives rise to a significant systematic uncertainty in our results. We further discuss this issue in Section 5.1.

3. INITIAL CONDITIONS

Here, we describe the initial conditions assumed in our simulations. We consider several sets of initial conditions; in each set, we generate $N_{\text{MC}} = 10^3$ systems through Monte Carlo sampling. Each set is characterized by the type of system – ‘Triple’ or ‘Binary’, where ‘Binary’ refers to the same system, but in absence of the tertiary star –, the dispersion σ_k assumed in the kick speed distribution (see equation 1), and the type of assumption on the tertiary mass distribution (see Section 3.1 below).

Below, we describe in more detail the assumptions made in the Monte Carlo sampling. An overview of our notation and assumptions is given in Table 1.

3.1. Masses

We sample the mass of the primary star, m_1 , from a Salpeter distribution (Salpeter 1955), i.e., $dN/dm_1 \propto m_1^{-2.35}$. Since our interest is in NS mergers, we sample with the range $8 < m_1/M_\odot < 50$. The mass of the secondary star, m_2 is sampled assuming a flat distribution in $q_1 \equiv m_2/m_1$, consistent with observations of massive stars (e.g., Sana et al. 2012; Duchêne & Kraus 2013; Kobulnicky et al. 2014). Here, we set the lower limit on m_2 to be $4 M_\odot$. The tertiary mass m_3 is sampled according to two methods: sampling from (1) a flat distribution in the mass ratio $q_2 \equiv m_3/(m_1 + m_2)$, and (2) a flat distribution in the mass ratio $q'_2 \equiv m_3/m_2$. In either case, we set the lower limit on m_3 to be $0.1 M_\odot$. These two choices give different results in our simulations, since in case (1) the tertiary star can be more massive than the primary star, and therefore can evolve first. Consequently, the tertiary star can become unbound from the inner binary as it explodes in a SNe event. In contrast, in method (2), the tertiary star is always less massive than the primary star, such that the inner binary always evolves first.

In Fig. 1, we illustrate the difference between the two assumptions on the tertiary mass ratio distribution. With method (1), the median tertiary mass is $\approx 5 M_\odot$, whereas with method (2) it is $\approx 12 M_\odot$.

3.2. Orbits

For both inner and outer orbits, we assume a flat distribution in the logarithm of the orbital period, i.e., flat in $\log_{10}(P_{\text{orb},i})$ (also known as an Öpik distribution, Öpik 1924). The limits for both inner and outer orbits are set to $1 < \log_{10}(P_{\text{orb},i}/\text{d}) <$

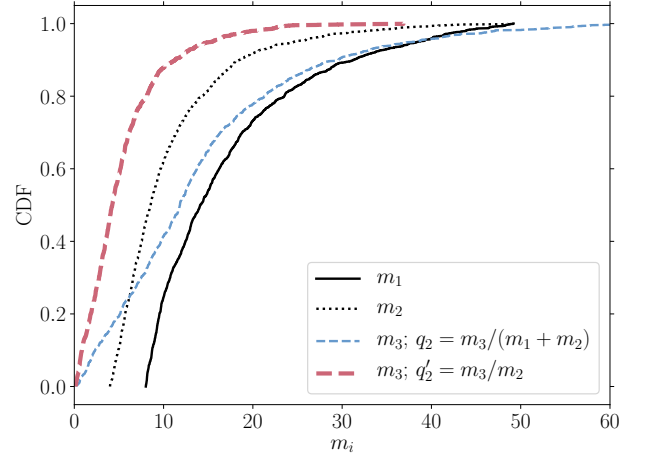


Figure 1. Distributions of the initial primary, secondary, and tertiary masses in the Monte Carlo simulations. The thin (thick) dashed lines show the distributions of the tertiary mass m_3 assuming method 1 (2) for the tertiary mass ratio q_2 (q'_2).

10. The eccentricities e_i of both inner and outer orbits are sampled from flat distributions in e_i , with $0 < e_j < 0.9$. The orbital period and eccentricity distributions are roughly consistent with observations of massive binary stars (Kobulnicky et al. 2014). Given the uncertainties in the observed orbital distributions of massive triples, we do not take into account a more sophisticated initial distribution, even though the observed distribution for massive MS triples reflects the initial distribution (Rose et al. 2019).

We reject a sampled system if it is unstable according to the criterion of Mardling & Aarseth (2001). The orientations of the orbits are taken to be random, i.e., the inclinations i_i are sampled from flat distributions in $\cos i_i$, and the arguments of periastris ω_i and longitudes of the ascending node Ω_i are sampled from flat distributions. There are indications that lower-mass triples have more aligned inner and outer orbits if the system is compact ($a_2 \lesssim 100 \text{ AU}$), whereas the wider systems are more isotropically distributed (Tokovinin 2017). However, it is unclear if this trend also persists for higher-mass triples (primaries with masses $\gtrsim 8 M_\odot$). For simplicity, we here restrict to randomly-oriented triples.

3.3. Kick distributions

As discussed in Section 2, we sample the kick distribution for SNe from a Maxwellian distribution (e.g., Hansen & Phinney 1997). We take the dispersion σ_k to be fixed for each set of Monte Carlo simulations, and adopt three values: 0, 40, and 265 km s^{-1} . The value $\sigma_k = 0 \text{ km s}^{-1}$ is to evaluate the importance of mass loss associated with SNe only (i.e., only the Blaauw kick, Blaauw 1961; Boersma 1961). The value $\sigma_k = 265 \text{ km s}^{-1}$ is a commonly-adopted value inferred from the proper motions of pulsars (Hobbs et al. 2005). However, NS kicks are uncertain and their magnitude is still highly debated. For example, Arzoumanian et al. (2002) found a two-component distribution of kick speed distributions with characteristic velocities of 90 and 500 km s^{-1} based on the velocities of isolated radio pulsars, and Beniamini & Piran (2016) also found evidence for a bimodal distribution based on observed binary NSs, with a low-kick population with $V_k < 30 \text{ km s}^{-1}$, and a high-kick population with kicks up to 400 km s^{-1} . Rather than adopting a bimodal distribution, we

Symbol	Description	Initial value(s) and/or distribution in population synthesis
m_1	Mass of the primary star.	$8 - 50 M_\odot$ with a Salpeter initial mass function (Salpeter 1955, i.e., $dN/dm_1 \propto m_1^{-2.35}$).
m_2	Mass of the secondary star.	$m_1 q_1$, where q_1 has a flat distribution, and with $m_2 > 4 M_\odot$.
m_3	Mass of the tertiary star.	Either (1) $m_3 = q_2(m_1 + m_2)$, or (2) $m_3 = q'_2 m_2$, where both q_2 and q'_2 have a flat distribution, subject to $m_3 > 0.1 M_\odot$.
Z_i	Metallicity of star i .	0.02
R_i	Radius of star i .	From stellar evolution code.
$P_{s,i}$	Spin period of star i .	10 d
$\theta_{s,i}$	Obliquity (spin-orbit angle) of star i .	0°
$t_{V,i}$	Viscous time-scale of star i .	Computed from the stellar properties using the prescription of Hurley et al. (2002).
$k_{AM,i}$	Apsidal motion constant of star i .	0.014
$r_{g,i}$	Gyration radius of star i .	0.08
V_k	SNe kick speed.	Maxwellian distribution with $\sigma_k = 0, 40$, or 265 km s^{-1} .
$P_{orb,i}$	Orbital period of orbit i (inner orbit: $i = 1$; outer orbit: $i = 2$).	Flat distribution in $\log_{10}(P_{orb,i})$, with $1 < \log_{10}(P_{orb,i}/\text{d}) < 10$, and subject to dynamical stability constraints.
a_i	Semimajor axis of orbit i .	Computed from $P_{orb,i}$ and the m_i using Kepler's law.
e_i	Eccentricity of orbit i .	Flat distribution between 0 and 0.9.
i_i	Inclination of orbit i .	$0 - 180^\circ$ (flat distribution in $\cos i_i$)
ω_i	Argument of periastris of orbit i .	$0 - 360^\circ$ (flat distribution in ω_i)
Ω_i	Longitude of the ascending node of orbit i .	$0 - 360^\circ$ (flat distribution in Ω_i)

Table 1

Description of important quantities and their initial value(s) and/or distributions assumed in the population synthesis.

here choose to carry out another set with $\sigma_k = 40 \text{ km s}^{-1}$, to evaluate the importance of low but non-zero kicks.

4. RESULTS

4.1. Outcome fractions

4.1.1. Main channels

In Tables 2 and 3, we show the fractions for the main channels in our simulations assuming a flat distribution in $q_2 \equiv m_3/(m_1 + m_2)$ and $q'_2 \equiv m_3/m_2$, respectively (henceforth, we refer to the latter two assumptions on the tertiary mass ratio as the ‘high mass tertiary’ and ‘low mass tertiary’ cases, respectively). These data are based on simulations with SECULARMULTIPLE only. The first three data columns correspond to triple systems, whereas the last three data columns correspond to the binary case, i.e., taking the same triple systems but in the absence of the tertiary star. For each case, we show results for the three different values of the kick velocity dispersion, σ_k .

The channels shown in these tables include ‘No interaction’, i.e., the triple or binary survived for 10 Gyr without triggering interaction such as mass transfer, or dynamical instability or instability as a result of SNe. In most cases, this ‘inert’ channel is unlikely; instead, much more common are RLOF, or the unbinding of the system due to SNe. The only notable exception is for the binary case with $\sigma_k = 0 \text{ km s}^{-1}$, in which case the non-interacting fraction is ~ 0.2 . In the equivalent triple case, the non-interacting fraction is only ~ 0.02 , i.e., a factor 10 times smaller. This can be attributed largely due to the Blaauw kick in the inner binary which can keep the inner binary bound, but make the tertiary unbound (compare the ‘NS+MS’ Unbound fractions between the triple and binary cases with $\sigma_k = 0 \text{ km s}^{-1}$).

For RLOF, we distinguish between RLOF of the primary, secondary, or tertiary star (in the latter case, the inner binary is treated as a point mass in the fits of Sepinsky et al. 2007). RLOF is predominantly triggered by the primary star, with a fraction of ~ 0.6 assuming $\sigma_k = 0 \text{ km s}^{-1}$, and ~ 0.4 assuming $\sigma_k > 0 \text{ km s}^{-1}$ for the triple systems with higher-mass tertiaries. The decrease in the RLOF fraction with increasing σ_k in the latter case can be ascribed to the higher fraction of unbound systems, which in turn is mostly due to kicks im-

parted on the tertiary star when it evolves first (see the unbound MS+MS fractions for triples in Table 2). This trend is much less pronounced in the case of lower-mass tertiaries (Table 3) – in this case, the tertiary, which is always as massive or less massive than the secondary star, does not evolve first, and therefore is less likely to unbind the triple system due to its SNe kick.

In contrast to triples, for binaries, the RLOF star 1 fraction is independent of σ_k . This can be explained by noting that for binaries, the primary star is always the most massive and evolves the fastest; whether or not star fills its Roche lobe is completely determined by the initial masses (m_1 and m_2), a_1 , and e_1 , and independent of σ_k . This is no longer the case for the secondary star, e.g., RLOF of the secondary star can be triggered by a SNe event of the primary star, whose properties in turn are set by σ_k .

It may be surprising that the RLOF fraction is typically ~ 0.6 , for both triple and binary cases. It might be expected that the RLOF fraction would be much higher for triple systems, since RLOF can be triggered by LK evolution. To explain this, we note that in most previous studies of the onset of RLOF in triples (e.g., Hamers et al. 2013; Antonini et al. 2017; Hamers & Thompson 2019), the inner binaries were assumed to be wide enough to avoid interaction in the absence of a tertiary star. In contrast, we here include tight systems as well. Therefore, a significant fraction of systems already interact in the ‘binary case’. In addition, as shown by the higher unbound fractions for the triple cases compared to the binary cases, orbital changes due to SNe associated with the tertiary star play an important role in triples with NSs.

The fraction of dynamically unstable systems for triples is relatively small, with the fraction being at most ~ 0.03 if $\sigma_k = 0 \text{ km s}^{-1}$. Dynamical instability is typically triggered by mass loss from the inner binary, i.e., the traditional triple dynamical instability scenario (Perets & Kratter 2012). Instability can also be triggered by SNe events, but this is a rare event. The dynamical instability fraction in fact decreases with increasing σ_k , which can be understood from the larger fraction of systems becoming unbound due to SNe before a dynamical instability can be triggered.

As discussed in Section 2, we also check for the semisecular

	Fraction of all systems					
	Triple			Binary		
	0	$\sigma_k/\text{km s}^{-1}$ 40	265	0	$\sigma_k/\text{km s}^{-1}$ 40	265
No Interaction	0.024 ± 0.005	0.004 ± 0.002	0.004 ± 0.002	0.253 ± 0.016	0.011 ± 0.003	0.008 ± 0.003
RLOF ★1	0.607 ± 0.025	0.445 ± 0.021	0.442 ± 0.021	0.612 ± 0.025	0.612 ± 0.025	0.612 ± 0.025
MS	0.068 ± 0.008	0.063 ± 0.008	0.061 ± 0.008	0.056 ± 0.007	0.056 ± 0.007	0.056 ± 0.007
G	0.444 ± 0.021	0.314 ± 0.018	0.313 ± 0.018	0.460 ± 0.021	0.460 ± 0.021	0.460 ± 0.021
CHeB	0.095 ± 0.010	0.068 ± 0.008	0.068 ± 0.008	0.096 ± 0.010	0.096 ± 0.010	0.096 ± 0.010
RLOF ★2	0.024 ± 0.005	0.021 ± 0.005	0.021 ± 0.005	0.021 ± 0.005	0.009 ± 0.003	0.002 ± 0.001
MS	0.021 ± 0.005	0.021 ± 0.005	0.021 ± 0.005	0.000 ± 0.000	0.000 ± 0.000	0.000 ± 0.000
G	0.002 ± 0.001	0.000 ± 0.000	0.000 ± 0.000	0.021 ± 0.005	0.009 ± 0.003	0.002 ± 0.001
CHeB	0.001 ± 0.001	0.000 ± 0.000	0.000 ± 0.000	0.000 ± 0.000	0.000 ± 0.000	0.000 ± 0.000
RLOF ★3	0.009 ± 0.003	0.009 ± 0.003	0.008 ± 0.003	—	—	—
MS	0.000 ± 0.000	0.000 ± 0.000	0.000 ± 0.000	—	—	—
G	0.004 ± 0.002	0.004 ± 0.002	0.004 ± 0.002	—	—	—
CHeB	0.005 ± 0.002	0.005 ± 0.002	0.004 ± 0.002	—	—	—
Dynamical inst.	0.028 ± 0.005	0.003 ± 0.002	0.004 ± 0.002	—	—	—
MS+MS	0.002 ± 0.001	0.002 ± 0.001	0.003 ± 0.002	—	—	—
G+MS	0.000 ± 0.000	0.000 ± 0.000	0.000 ± 0.000	—	—	—
CHeB+MS	0.000 ± 0.000	0.000 ± 0.000	0.000 ± 0.000	—	—	—
NS+MS	0.012 ± 0.003	0.000 ± 0.000	0.000 ± 0.000	—	—	—
NS+G	0.003 ± 0.002	0.000 ± 0.000	0.000 ± 0.000	—	—	—
NS+CHeB	0.003 ± 0.002	0.000 ± 0.000	0.000 ± 0.000	—	—	—
NS+NS	0.000 ± 0.000	0.000 ± 0.000	0.000 ± 0.000	—	—	—
BH+MS	0.004 ± 0.002	0.000 ± 0.000	0.000 ± 0.000	—	—	—
BH+G	0.001 ± 0.001	0.000 ± 0.000	0.000 ± 0.000	—	—	—
BH+CHeB	0.001 ± 0.001	0.001 ± 0.001	0.001 ± 0.001	—	—	—
BH+NS	0.002 ± 0.001	0.000 ± 0.000	0.000 ± 0.000	—	—	—
BH+BH	0.000 ± 0.000	0.000 ± 0.000	0.000 ± 0.000	—	—	—
Semiseccular	0.004 ± 0.002	0.004 ± 0.002	0.004 ± 0.002	—	—	—
MS+MS	0.004 ± 0.002	0.004 ± 0.002	0.004 ± 0.002	—	—	—
Secular collision	0.000 ± 0.000	0.000 ± 0.000	0.000 ± 0.000	0.000 ± 0.000	0.000 ± 0.000	0.000 ± 0.000
MS+MS	0.000 ± 0.000	0.000 ± 0.000	0.000 ± 0.000	0.000 ± 0.000	0.000 ± 0.000	0.000 ± 0.000
Unbound (SNe)	0.304 ± 0.017	0.514 ± 0.023	0.517 ± 0.023	0.114 ± 0.011	0.368 ± 0.019	0.378 ± 0.019
MS+MS	0.000 ± 0.000	0.262 ± 0.016	0.265 ± 0.016	0.000 ± 0.000	0.000 ± 0.000	0.000 ± 0.000
G+MS	0.000 ± 0.000	0.004 ± 0.002	0.004 ± 0.002	0.000 ± 0.000	0.000 ± 0.000	0.000 ± 0.000
CHeB+MS	0.000 ± 0.000	0.017 ± 0.004	0.017 ± 0.004	0.000 ± 0.000	0.000 ± 0.000	0.000 ± 0.000
NS+MS	0.219 ± 0.015	0.136 ± 0.012	0.136 ± 0.012	0.024 ± 0.005	0.263 ± 0.016	0.269 ± 0.016
NS+G	0.000 ± 0.000	0.001 ± 0.001	0.001 ± 0.001	0.000 ± 0.000	0.001 ± 0.001	0.001 ± 0.001
NS+CHeB	0.022 ± 0.005	0.020 ± 0.004	0.020 ± 0.004	0.000 ± 0.000	0.029 ± 0.005	0.029 ± 0.005
NS+NS	0.007 ± 0.003	0.000 ± 0.000	0.000 ± 0.000	0.084 ± 0.009	0.001 ± 0.001	0.000 ± 0.000
BH+MS	0.019 ± 0.004	0.056 ± 0.007	0.056 ± 0.007	0.000 ± 0.000	0.046 ± 0.007	0.054 ± 0.007
BH+G	0.000 ± 0.000	0.000 ± 0.000	0.000 ± 0.000	0.000 ± 0.000	0.000 ± 0.000	0.000 ± 0.000
BH+CHeB	0.001 ± 0.001	0.005 ± 0.002	0.005 ± 0.002	0.000 ± 0.000	0.004 ± 0.002	0.004 ± 0.002
BH+NS	0.028 ± 0.005	0.005 ± 0.002	0.005 ± 0.002	0.006 ± 0.002	0.014 ± 0.004	0.010 ± 0.003
BH+BH	0.008 ± 0.003	0.008 ± 0.003	0.008 ± 0.003	0.000 ± 0.000	0.010 ± 0.003	0.011 ± 0.003
Inner bound	0.286 ± 0.017	0.304 ± 0.017	0.295 ± 0.017	—	—	—

Table 2

Outcome fractions of the simulations with the tertiary mass assuming a flat distribution in $q_2 \equiv m_3/(m_1 + m_2)$. The first three data columns correspond to triple systems, whereas the last three data columns correspond to the binary case, i.e., taking the same triple systems but in the absence of the tertiary star. For each case, we show results for the three different values of the kick velocity dispersion, σ_k . Fractions are based on $N_{\text{MC}} = 10^3$ simulations, and quoted errors are based on Poisson statistics. Outcomes that do not apply (e.g., dynamically unstable systems in the binary case) are marked with ‘—’. Some of the stellar evolutionary states are G – giant star (including red giants and asymptotic giants), and core helium burning star (CHeB). Refer to the text in Section 4.1.1 for a description of the different channels.

regime in our simulations. This regime is triggered only very rarely, and predominantly with the inner binary consisting of two MS stars. The reason for the rarity of this channel is that very high eccentricities are required to trigger it, which usually instead lead to RLOF in eccentric orbits.

We also check for direct collisions (indicated with ‘Secular collision’ in the tables). These do not occur for pre-compact objects, since RLOF is expected to ensue before direct collision. However, direct collisions could occur during later stages, when compact objects have formed, and when the inner orbit is excited in eccentricity due to secular evolution (e.g., Thompson 2011; Katz & Dong 2012). Nevertheless, we find no such direct collisions of compact objects. This can be

attributed to the high fractions of systems that undergo RLOF or become unbound. In other words, the probability that the system survives without interacting or becoming unstable due to SNe and a collision is triggered at later stages, is small. We emphasize that our simulations are limited in terms of the number of systems. We therefore cannot exclude that direct collisions would occur if N_{MC} were increased. However, we here focus on the largest contribution to NS-NS mergers, which we find originate from interacting or unbound systems (i.e., RLOF-induced and ‘unbound’ mergers). The latter are discussed in further detail below.

4.1.2. Mergers from RLOF systems

	Fraction of all systems					
	Triple			Binary		
	0	$\sigma_k/\text{km s}^{-1}$ 40	265	0	$\sigma_k/\text{km s}^{-1}$ 40	265
No Interaction	0.026 ± 0.005	0.006 ± 0.002	0.006 ± 0.002	0.221 ± 0.015	0.011 ± 0.003	0.008 ± 0.003
RLOF ★1	0.618 ± 0.025	0.622 ± 0.025	0.621 ± 0.025	0.595 ± 0.024	0.612 ± 0.025	0.612 ± 0.025
MS	0.060 ± 0.008	0.060 ± 0.008	0.061 ± 0.008	0.056 ± 0.007	0.056 ± 0.007	0.056 ± 0.007
G	0.457 ± 0.021	0.462 ± 0.021	0.460 ± 0.021	0.448 ± 0.021	0.460 ± 0.021	0.460 ± 0.021
CHeB	0.101 ± 0.010	0.100 ± 0.010	0.100 ± 0.010	0.091 ± 0.010	0.096 ± 0.010	0.096 ± 0.010
RLOF ★2	0.017 ± 0.004	0.016 ± 0.004	0.016 ± 0.004	0.018 ± 0.004	0.004 ± 0.002	0.002 ± 0.001
MS	0.014 ± 0.004	0.014 ± 0.004	0.014 ± 0.004	0.000 ± 0.000	0.001 ± 0.001	0.000 ± 0.000
G	0.002 ± 0.001	0.002 ± 0.001	0.002 ± 0.001	0.018 ± 0.004	0.003 ± 0.002	0.002 ± 0.001
CHeB	0.001 ± 0.001	0.000 ± 0.000	0.000 ± 0.000	0.000 ± 0.000	0.000 ± 0.000	0.000 ± 0.000
RLOF ★3	0.000 ± 0.000	0.000 ± 0.000	0.000 ± 0.000	—	—	—
MS	0.000 ± 0.000	0.000 ± 0.000	0.000 ± 0.000	—	—	—
G	0.000 ± 0.000	0.000 ± 0.000	0.000 ± 0.000	—	—	—
CHeB	0.000 ± 0.000	0.000 ± 0.000	0.000 ± 0.000	—	—	—
Dynamical inst.	0.035 ± 0.006	0.006 ± 0.002	0.005 ± 0.002	—	—	—
MS+MS	0.004 ± 0.002	0.004 ± 0.002	0.004 ± 0.002	—	—	—
G+MS	0.000 ± 0.000	0.000 ± 0.000	0.000 ± 0.000	—	—	—
CHeB+MS	0.000 ± 0.000	0.000 ± 0.000	0.000 ± 0.000	—	—	—
NS+MS	0.013 ± 0.004	0.000 ± 0.000	0.000 ± 0.000	—	—	—
NS+G	0.005 ± 0.002	0.000 ± 0.000	0.000 ± 0.000	—	—	—
NS+CHeB	0.002 ± 0.001	0.000 ± 0.000	0.000 ± 0.000	—	—	—
NS+NS	0.001 ± 0.001	0.000 ± 0.000	0.000 ± 0.000	—	—	—
BH+MS	0.005 ± 0.002	0.001 ± 0.001	0.000 ± 0.000	—	—	—
BH+G	0.001 ± 0.001	0.000 ± 0.000	0.000 ± 0.000	—	—	—
BH+CHeB	0.002 ± 0.001	0.001 ± 0.001	0.001 ± 0.001	—	—	—
BH+NS	0.002 ± 0.001	0.000 ± 0.000	0.000 ± 0.000	—	—	—
BH+BH	0.000 ± 0.000	0.000 ± 0.000	0.000 ± 0.000	—	—	—
Semiseccular	0.003 ± 0.002	0.002 ± 0.001	0.002 ± 0.001	—	—	—
MS+MS	0.002 ± 0.001	0.002 ± 0.001	0.002 ± 0.001	—	—	—
Secular collision	0.000 ± 0.000	0.000 ± 0.000	0.000 ± 0.000	0.000 ± 0.000	0.000 ± 0.000	0.000 ± 0.000
MS+MS	0.000 ± 0.000	0.000 ± 0.000	0.000 ± 0.000	0.000 ± 0.000	0.000 ± 0.000	0.000 ± 0.000
Unbound (SNe)	0.301 ± 0.017	0.348 ± 0.019	0.350 ± 0.019	0.160 ± 0.013	0.373 ± 0.019	0.378 ± 0.019
MS+MS	0.000 ± 0.000	0.000 ± 0.000	0.000 ± 0.000	0.000 ± 0.000	0.000 ± 0.000	0.000 ± 0.000
G+MS	0.000 ± 0.000	0.000 ± 0.000	0.000 ± 0.000	0.000 ± 0.000	0.000 ± 0.000	0.000 ± 0.000
CHeB+MS	0.000 ± 0.000	0.000 ± 0.000	0.000 ± 0.000	0.000 ± 0.000	0.000 ± 0.000	0.000 ± 0.000
NS+MS	0.218 ± 0.015	0.245 ± 0.016	0.245 ± 0.016	0.048 ± 0.007	0.266 ± 0.016	0.268 ± 0.016
NS+G	0.000 ± 0.000	0.001 ± 0.001	0.001 ± 0.001	0.000 ± 0.000	0.001 ± 0.001	0.001 ± 0.001
NS+CHeB	0.024 ± 0.005	0.028 ± 0.005	0.028 ± 0.005	0.000 ± 0.000	0.028 ± 0.005	0.029 ± 0.005
NS+NS	0.009 ± 0.003	0.000 ± 0.000	0.000 ± 0.000	0.099 ± 0.010	0.001 ± 0.001	0.000 ± 0.000
BH+MS	0.020 ± 0.004	0.050 ± 0.007	0.053 ± 0.007	0.003 ± 0.002	0.048 ± 0.007	0.055 ± 0.007
BH+G	0.000 ± 0.000	0.000 ± 0.000	0.000 ± 0.000	0.000 ± 0.000	0.000 ± 0.000	0.000 ± 0.000
BH+CHeB	0.000 ± 0.000	0.004 ± 0.002	0.004 ± 0.002	0.000 ± 0.000	0.004 ± 0.002	0.004 ± 0.002
BH+NS	0.026 ± 0.005	0.008 ± 0.003	0.008 ± 0.003	0.009 ± 0.003	0.012 ± 0.003	0.010 ± 0.003
BH+BH	0.004 ± 0.002	0.012 ± 0.003	0.011 ± 0.003	0.001 ± 0.001	0.013 ± 0.004	0.011 ± 0.003
Inner bound	0.269 ± 0.016	0.012 ± 0.001	0.003 ± 0.002	—	—	—

Table 3

Similar to Table 2, here for simulations with the tertiary mass sampled assuming a flat distribution in $q'_2 \equiv m_3/m_2$.

As described in detail in Section 2.2, we continue the evolution of the inner binary after RLOF occurs in the inner binary using the binary population synthesis code BSE. In Tables 4 and 5 for the high- and low-mass tertiary simulations, respectively, we show the fractions for merger outcomes of the subsequent ‘isolated binary’ simulations. These fractions are with respect to the systems undergoing RLOF triggered by the primary or secondary star; the fractions of the latter cases corresponding to *all* systems were given in Tables 2 and 3 for the high- and low-mass tertiary cases, respectively.

The evolution of the inner binary after RLOF in BSE is driven by several processes, including mass transfer, CE evolution, and SNe. There is a high likelihood, of ~ 0.7 to ~ 0.9 of the RLOF systems depending on σ_k , that the inner binary eventually merges. It is evident from Tables 4 and 5 that a large number of merger outcomes are possible. Generally, there are little differences in the fractions between the ‘triple’

and ‘binary’ cases. This can be attributed to the generally only small differences in the properties of the inner binaries when RLOF is triggered (see Section 4.2 below).

A dominant merger channel is a NS-MS merger, with a fraction of up to ~ 0.6 of RLOF systems if $\sigma_k = 265 \text{ km s}^{-1}$. The resulting stars, Thorne-Żytkow objects (Thorne & Żytkow 1977), are also found in isolated binary evolution studies (e.g., Brandt & Podsiadlowski 1995); our results show that this channel is also possible (and relatively likely) in triples. These objects could also evolve to become X-ray binaries, which are also believed to form in triples (without taking into account isolated binary evolution) through the mass-loss induced eccentric LK mechanism (Shappee & Thompson 2013; Naoz et al. 2016).

The channel of most interest here is the merger of two NSs, which occurs for a relatively large fraction of ~ 0.1 of RLOF systems if $\sigma_k = 0 \text{ km s}^{-1}$, but drops quickly to a tenth of this

	Fraction of RLOF systems (★1 or ★2)					
	Triple			Binary		
	0	$\sigma_k/\text{km s}^{-1}$ 40	265	0	$\sigma_k/\text{km s}^{-1}$ 40	265
RLOF → Merger	0.743 ± 0.034	0.835 ± 0.042	0.905 ± 0.044	0.708 ± 0.033	0.842 ± 0.037	0.914 ± 0.039
MS+MS	0.079 ± 0.011	0.101 ± 0.015	0.102 ± 0.015	0.039 ± 0.008	0.040 ± 0.008	0.041 ± 0.008
CHeB+MS	0.035 ± 0.007	0.030 ± 0.008	0.032 ± 0.008	0.021 ± 0.006	0.021 ± 0.006	0.020 ± 0.006
CHeB+G	0.005 ± 0.003	0.004 ± 0.003	0.004 ± 0.003	0.003 ± 0.002	0.003 ± 0.002	0.003 ± 0.002
G+MS	0.052 ± 0.009	0.052 ± 0.011	0.052 ± 0.011	0.063 ± 0.010	0.064 ± 0.010	0.065 ± 0.010
G+CHeB	0.000 ± 0.000	0.000 ± 0.000	0.000 ± 0.000	0.000 ± 0.000	0.000 ± 0.000	0.000 ± 0.000
G+G	0.000 ± 0.000	0.000 ± 0.000	0.000 ± 0.000	0.000 ± 0.000	0.000 ± 0.000	0.000 ± 0.000
He+MS	0.016 ± 0.005	0.002 ± 0.002	0.004 ± 0.003	0.011 ± 0.004	0.011 ± 0.004	0.016 ± 0.005
He+G	0.005 ± 0.003	0.004 ± 0.003	0.004 ± 0.003	0.003 ± 0.002	0.003 ± 0.002	0.003 ± 0.002
WD+MS	0.073 ± 0.011	0.049 ± 0.010	0.050 ± 0.010	0.070 ± 0.010	0.072 ± 0.011	0.073 ± 0.011
WD+G	0.013 ± 0.004	0.017 ± 0.006	0.017 ± 0.006	0.022 ± 0.006	0.021 ± 0.006	0.021 ± 0.006
WD+He	0.002 ± 0.002	0.000 ± 0.000	0.002 ± 0.002	0.006 ± 0.003	0.006 ± 0.003	0.008 ± 0.004
WD+WD	0.002 ± 0.002	0.004 ± 0.003	0.004 ± 0.003	0.000 ± 0.000	0.000 ± 0.000	0.000 ± 0.000
NS+MS	0.209 ± 0.018	0.423 ± 0.030	0.576 ± 0.035	0.207 ± 0.018	0.417 ± 0.026	0.578 ± 0.031
NS+CHeB	0.011 ± 0.004	0.006 ± 0.004	0.004 ± 0.003	0.032 ± 0.007	0.011 ± 0.004	0.008 ± 0.004
NS+G	0.082 ± 0.011	0.047 ± 0.010	0.000 ± 0.000	0.073 ± 0.011	0.047 ± 0.009	0.008 ± 0.004
NS+He	0.016 ± 0.005	0.006 ± 0.004	0.004 ± 0.003	0.017 ± 0.005	0.014 ± 0.005	0.005 ± 0.003
NS+WD	0.013 ± 0.004	0.009 ± 0.004	0.002 ± 0.002	0.008 ± 0.004	0.005 ± 0.003	0.003 ± 0.002
NS+NS	0.105 ± 0.013	0.045 ± 0.010	0.009 ± 0.004	0.104 ± 0.013	0.058 ± 0.010	0.015 ± 0.005
BH+MS	0.008 ± 0.004	0.011 ± 0.005	0.013 ± 0.005	0.011 ± 0.004	0.011 ± 0.004	0.011 ± 0.004
BH+CHeB	0.000 ± 0.000	0.000 ± 0.000	0.000 ± 0.000	0.000 ± 0.000	0.000 ± 0.000	0.000 ± 0.000
BH+G	0.000 ± 0.000	0.000 ± 0.000	0.000 ± 0.000	0.002 ± 0.002	0.002 ± 0.002	0.002 ± 0.002
BH+He	0.000 ± 0.000	0.000 ± 0.000	0.000 ± 0.000	0.000 ± 0.000	0.000 ± 0.000	0.000 ± 0.000
BH+WD	0.000 ± 0.000	0.000 ± 0.000	0.000 ± 0.000	0.000 ± 0.000	0.000 ± 0.000	0.000 ± 0.000
BH+NS	0.010 ± 0.004	0.021 ± 0.007	0.022 ± 0.007	0.005 ± 0.003	0.023 ± 0.006	0.021 ± 0.006
BH+BH	0.002 ± 0.002	0.002 ± 0.002	0.002 ± 0.002	0.002 ± 0.002	0.002 ± 0.002	0.002 ± 0.002
Other	0.008 ± 0.004	0.000 ± 0.000	0.000 ± 0.000	0.009 ± 0.004	0.010 ± 0.004	0.010 ± 0.004

Table 4

Fractions for merger outcomes in the ‘isolated binary’ simulations, which are based on the systems in which RLOF was triggered in the inner binary system. Data in this table are based on the high-mass tertiary case, i.e., $m_3 = q_2(m_1 + m_2)$; see Table 5 for the low-mass tertiary case. The fractions in this table are given with respect to the systems undergoing RLOF triggered by the primary or secondary star; the fractions of the latter cases corresponding to *all* systems were given in Table 2. Here, ‘He’ refers to a helium-burning star.

	Fraction of RLOF systems (★1 or ★2)					
	Triple			Binary		
	0	$\sigma_k/\text{km s}^{-1}$ 40	265	0	$\sigma_k/\text{km s}^{-1}$ 40	265
RLOF → Merger	0.745 ± 0.034	0.843 ± 0.036	0.915 ± 0.038	0.711 ± 0.034	0.830 ± 0.037	0.909 ± 0.038
MS+MS	0.066 ± 0.010	0.066 ± 0.010	0.066 ± 0.010	0.041 ± 0.008	0.041 ± 0.008	0.041 ± 0.008
CHeB+MS	0.022 ± 0.006	0.017 ± 0.005	0.019 ± 0.005	0.018 ± 0.005	0.018 ± 0.005	0.015 ± 0.005
CHeB+G	0.003 ± 0.002	0.003 ± 0.002	0.005 ± 0.003	0.003 ± 0.002	0.003 ± 0.002	0.005 ± 0.003
G+MS	0.054 ± 0.009	0.061 ± 0.010	0.058 ± 0.010	0.055 ± 0.010	0.057 ± 0.010	0.055 ± 0.009
G+CHeB	0.000 ± 0.000	0.000 ± 0.000	0.000 ± 0.000	0.000 ± 0.000	0.000 ± 0.000	0.000 ± 0.000
G+G	0.000 ± 0.000	0.000 ± 0.000	0.000 ± 0.000	0.000 ± 0.000	0.000 ± 0.000	0.000 ± 0.000
He+MS	0.017 ± 0.005	0.019 ± 0.005	0.020 ± 0.006	0.010 ± 0.004	0.016 ± 0.005	0.013 ± 0.005
He+G	0.009 ± 0.004	0.009 ± 0.004	0.008 ± 0.004	0.003 ± 0.002	0.003 ± 0.002	0.005 ± 0.003
WD+MS	0.068 ± 0.010	0.067 ± 0.010	0.072 ± 0.011	0.072 ± 0.011	0.081 ± 0.011	0.072 ± 0.011
WD+G	0.022 ± 0.006	0.019 ± 0.005	0.020 ± 0.006	0.024 ± 0.006	0.019 ± 0.006	0.021 ± 0.006
WD+He	0.006 ± 0.003	0.006 ± 0.003	0.006 ± 0.003	0.003 ± 0.002	0.003 ± 0.002	0.007 ± 0.003
WD+WD	0.000 ± 0.000	0.000 ± 0.000	0.000 ± 0.000	0.000 ± 0.000	0.000 ± 0.000	0.000 ± 0.000
NS+MS	0.217 ± 0.018	0.411 ± 0.025	0.570 ± 0.030	0.212 ± 0.019	0.409 ± 0.026	0.596 ± 0.031
NS+CHeB	0.024 ± 0.006	0.006 ± 0.003	0.002 ± 0.002	0.034 ± 0.007	0.015 ± 0.005	0.008 ± 0.004
NS+G	0.076 ± 0.011	0.050 ± 0.009	0.003 ± 0.002	0.077 ± 0.011	0.060 ± 0.010	0.005 ± 0.003
NS+He	0.016 ± 0.005	0.009 ± 0.004	0.006 ± 0.003	0.018 ± 0.005	0.006 ± 0.003	0.003 ± 0.002
NS+WD	0.013 ± 0.004	0.013 ± 0.004	0.006 ± 0.003	0.005 ± 0.003	0.010 ± 0.004	0.003 ± 0.002
NS+NS	0.107 ± 0.013	0.050 ± 0.009	0.017 ± 0.005	0.106 ± 0.013	0.044 ± 0.008	0.016 ± 0.005
BH+MS	0.011 ± 0.004	0.011 ± 0.004	0.011 ± 0.004	0.011 ± 0.004	0.011 ± 0.004	0.011 ± 0.004
BH+CHeB	0.000 ± 0.000	0.000 ± 0.000	0.000 ± 0.000	0.000 ± 0.000	0.000 ± 0.000	0.000 ± 0.000
BH+G	0.000 ± 0.000	0.002 ± 0.002	0.000 ± 0.000	0.002 ± 0.002	0.002 ± 0.002	0.002 ± 0.002
BH+He	0.002 ± 0.002	0.000 ± 0.000	0.000 ± 0.000	0.000 ± 0.000	0.000 ± 0.000	0.000 ± 0.000
BH+WD	0.000 ± 0.000	0.000 ± 0.000	0.000 ± 0.000	0.000 ± 0.000	0.000 ± 0.000	0.000 ± 0.000
BH+NS	0.006 ± 0.003	0.019 ± 0.005	0.019 ± 0.005	0.007 ± 0.003	0.019 ± 0.006	0.021 ± 0.006
BH+BH	0.002 ± 0.002	0.000 ± 0.000	0.002 ± 0.002	0.000 ± 0.000	0.002 ± 0.002	0.002 ± 0.002
Other	0.005 ± 0.003	0.005 ± 0.003	0.005 ± 0.003	0.010 ± 0.004	0.010 ± 0.004	0.008 ± 0.004

Table 5

Similar to Table 4, here based on the lower-mass-tertiary simulations.

fraction, to ~ 0.01 , if $\sigma_k = 265 \text{ km s}^{-1}$. As expected, the kick dispersion has a large impact on the fraction of NS-NS mergers. Also, these fraction are mostly sensitive to σ_k , and do not depend very strongly on the assumption of the tertiary mass ratio distribution (it should be taken into account, however, that the latter does affect the overall fraction of RLOF systems).

4.1.3. Mergers from systems with unbound tertiaries

In addition to considering the subsequent ‘isolated binary’ evolution of systems that undergo RLOF, we also consider the ‘isolated binary’ evolution of systems in which the tertiary becomes unbound from the system due to a SNe event, but the inner binary remains bound. In the latter case, the inner binary can subsequently merge due to ‘isolated binary’ evolution, which we take into account by evolving these systems with BSE (see Section 2.2). Similarly to Tables 4 and 5, we show in Tables 6 and 7 the outcome fractions of several merger channels for these ‘unbound tertiary’ systems. Evidently, in this case there are no equivalent ‘binary’ systems (since this channel originates exclusively from triples). The fractions in these tables are given with respect to the systems in which the tertiary becomes unbound, but with a bound inner binary; the latter fractions with respect to *all* systems are given in the bottom rows in Tables 2 and 3 for the high-mass and low-mass tertiaries, respectively. Note that the latter fraction is very small for the low-mass tertiary simulations and non-zero σ_k .

Similarly to RLOF-induced mergers, mergers originating from unbound tertiary systems are dominated by NS-MS mergers, in particular for non-zero σ_k . The fraction of NS-NS mergers is relatively high at ~ 0.25 for $\sigma_k = 0 \text{ km s}^{-1}$, but rapidly decreases with increasing σ_k , dropping to ~ 0.01 for $\sigma_k = 265 \text{ km s}^{-1}$ in the high-mass tertiary case, and to zero (within our statistical certainty) for $\sigma_k = 265 \text{ km s}^{-1}$ in the low-mass tertiary case.

4.2. Orbital properties

We further discuss the RLOF-induced (Section 4.1.2) and tertiary unbound (Section 4.1.3) channels by showing in Figs 2 and 3 the distributions of the inner binary semimajor axis a_1 and eccentricity e_1 at the moment of the onset of RLOF, and the unbinding of the tertiary star. Here, Figs 2 and 3 correspond to the high- and low-mass tertiary cases, respectively.

As expected, RLOF-induced systems tend to have significantly smaller inner binary semimajor axes compared to all systems (compare the red and black lines in the figures), with RLOF systems having a median of $a_1 \sim 1 \text{ AU}$, compared to $a_1 \sim 10 \text{ AU}$ for all systems overall. Also, SNe kicks have very little impact on the orbital properties RLOF systems, as expected (since in our simulations RLOF typically occurs before stars evolve to compact objects). In addition, for the RLOF systems there are little differences in terms of a_1 between the triple and binary cases. There is some difference in terms of the eccentricity – in the triple case, RLOF-induced systems tend to have slightly higher eccentricities compared to the binary case. This can be explained by eccentricity excitation by LK oscillations. There are no noticeable differences in the orbital properties of RLOF systems between the high- and low-mass tertiary simulations.

The ‘tertiary unbound’ systems show typically larger semimajor axes compared to all systems (compare the green and

	Fraction of unbound triples (stable inner binary) Triple		
	$\sigma_k / \text{km s}^{-1}$		
	0	40	265
Tertiary unbound			
→ inner binary merger	0.476 ± 0.041	0.931 ± 0.055	0.969 ± 0.057
MS+MS	0.000 ± 0.000	0.076 ± 0.016	0.078 ± 0.016
CHeB+MS	0.000 ± 0.000	0.003 ± 0.003	0.003 ± 0.003
CHeB+G	0.000 ± 0.000	0.000 ± 0.000	0.000 ± 0.000
G+MS	0.000 ± 0.000	0.023 ± 0.009	0.024 ± 0.009
G+CHeB	0.000 ± 0.000	0.000 ± 0.000	0.000 ± 0.000
G+G	0.000 ± 0.000	0.000 ± 0.000	0.000 ± 0.000
He+MS	0.000 ± 0.000	0.043 ± 0.012	0.041 ± 0.012
He+G	0.000 ± 0.000	0.003 ± 0.003	0.003 ± 0.003
WD+MS	0.000 ± 0.000	0.109 ± 0.019	0.112 ± 0.019
WD+G	0.000 ± 0.000	0.016 ± 0.007	0.017 ± 0.008
WD+He	0.000 ± 0.000	0.000 ± 0.000	0.000 ± 0.000
WD+WD	0.000 ± 0.000	0.000 ± 0.000	0.000 ± 0.000
NS+MS	0.164 ± 0.024	0.513 ± 0.041	0.600 ± 0.045
NS+CHeB	0.003 ± 0.003	0.036 ± 0.011	0.037 ± 0.011
NS+G	0.000 ± 0.000	0.026 ± 0.009	0.003 ± 0.003
NS+He	0.000 ± 0.000	0.007 ± 0.005	0.003 ± 0.003
NS+WD	0.000 ± 0.000	0.003 ± 0.003	0.000 ± 0.000
NS+NS	0.252 ± 0.030	0.013 ± 0.007	0.007 ± 0.005
BH+MS	0.000 ± 0.000	0.000 ± 0.000	0.000 ± 0.000
BH+CHeB	0.000 ± 0.000	0.000 ± 0.000	0.000 ± 0.000
BH+G	0.000 ± 0.000	0.000 ± 0.000	0.000 ± 0.000
BH+He	0.000 ± 0.000	0.000 ± 0.000	0.000 ± 0.000
BH+WD	0.000 ± 0.000	0.000 ± 0.000	0.000 ± 0.000
BH+NS	0.056 ± 0.014	0.053 ± 0.013	0.034 ± 0.011
BH+BH	0.000 ± 0.000	0.000 ± 0.000	0.000 ± 0.000
Other	0.000 ± 0.000	0.007 ± 0.005	0.007 ± 0.005

Table 6

Fractions for merger outcomes in the ‘isolated binary’ simulations, which are based on the systems in which the tertiary becomes unbound from the inner binary due to a SNe event. Data in this table are based on the high-mass tertiary case, i.e., $m_3 = q_2(m_1 + m_2)$; see Table 7 for the low-mass tertiary case. The fractions in this table are given with respect to the systems in which the tertiary becomes unbound, but with the inner binary still bound; the latter fraction is given in the last row of Table 2.

	Fraction of unbound triples (stable inner binary) Triple		
	$\sigma_k / \text{km s}^{-1}$		
	0	40	265
Tertiary unbound			
→ inner binary merger	0.513 ± 0.044	0.583 ± 0.220	0.333 ± 0.333
MS+MS	0.000 ± 0.000	0.000 ± 0.000	0.000 ± 0.000
CHeB+MS	0.000 ± 0.000	0.000 ± 0.000	0.000 ± 0.000
CHeB+G	0.000 ± 0.000	0.000 ± 0.000	0.000 ± 0.000
G+MS	0.000 ± 0.000	0.000 ± 0.000	0.000 ± 0.000
G+CHeB	0.000 ± 0.000	0.000 ± 0.000	0.000 ± 0.000
G+G	0.000 ± 0.000	0.000 ± 0.000	0.000 ± 0.000
He+MS	0.000 ± 0.000	0.000 ± 0.000	0.000 ± 0.000
He+G	0.000 ± 0.000	0.000 ± 0.000	0.000 ± 0.000
WD+MS	0.000 ± 0.000	0.000 ± 0.000	0.000 ± 0.000
WD+G	0.000 ± 0.000	0.000 ± 0.000	0.000 ± 0.000
WD+He	0.000 ± 0.000	0.000 ± 0.000	0.000 ± 0.000
WD+WD	0.000 ± 0.000	0.000 ± 0.000	0.000 ± 0.000
NS+MS	0.204 ± 0.028	0.333 ± 0.167	0.000 ± 0.000
NS+CHeB	0.000 ± 0.000	0.000 ± 0.000	0.000 ± 0.000
NS+G	0.000 ± 0.000	0.000 ± 0.000	0.000 ± 0.000
NS+He	0.000 ± 0.000	0.000 ± 0.000	0.000 ± 0.000
NS+WD	0.000 ± 0.000	0.000 ± 0.000	0.000 ± 0.000
NS+NS	0.242 ± 0.030	0.000 ± 0.000	0.000 ± 0.000
BH+MS	0.000 ± 0.000	0.000 ± 0.000	0.000 ± 0.000
BH+CHeB	0.000 ± 0.000	0.000 ± 0.000	0.000 ± 0.000
BH+G	0.000 ± 0.000	0.000 ± 0.000	0.000 ± 0.000
BH+He	0.000 ± 0.000	0.000 ± 0.000	0.000 ± 0.000
BH+WD	0.000 ± 0.000	0.000 ± 0.000	0.000 ± 0.000
BH+NS	0.067 ± 0.016	0.250 ± 0.144	0.333 ± 0.333
BH+BH	0.000 ± 0.000	0.000 ± 0.000	0.000 ± 0.000
Other	0.000 ± 0.000	0.000 ± 0.000	0.000 ± 0.000

Table 7

Similar to Table 6, here based on the lower-mass-tertiary simulations.

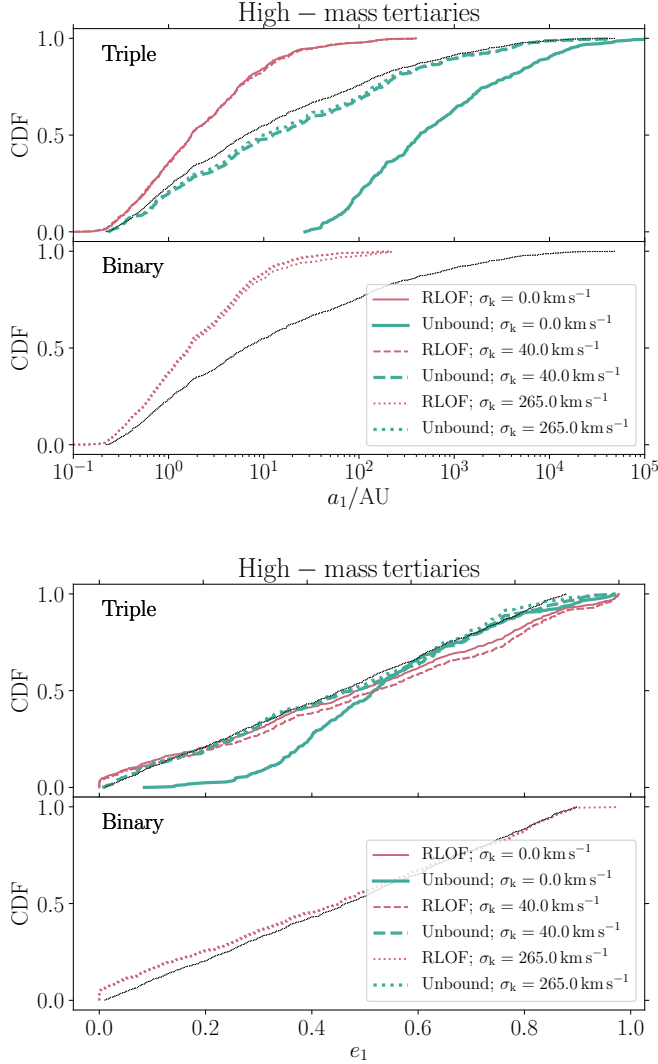


Figure 2. Distributions of the inner binary semimajor axis a_1 (top panels) and eccentricity e_1 (lower panels) at the moment of the onset of RLOF (thin red lines), and the unbinding of the tertiary star (thick green lines). In each set of panels, the top (bottom) panel corresponds to the triple (binary) case. Evidently, the ‘unbound tertiary’ channel does not apply in the binary case. Results here are shown for the high-mass tertiary simulations; refer to Fig. 3 for the low-mass tertiary case. Different line styles correspond to simulations with different σ_k : lines are solid, dashed and dotted for $\sigma_k = 0, 40$, and 265 km s^{-1} , respectively. The thin dotted black lines show the initial distributions of all systems in the simulations.

black lines in the figures). With higher kicks, the semimajor axes tend to be larger compared to without ($\sigma_k = 0 \text{ km s}^{-1}$); this can be understood by noting that kicks tend to unbind the inner binary if it is wide, so, for the inner binary to remain bound, the inner binary semimajor axis should be smaller. Note that the number of unbound systems in the low-mass tertiary simulations for $\sigma_k > 0 \text{ km s}^{-1}$ are very small (see the bottom row in Table 3), causing the jagged behavior in Fig. 3.

4.3. Delay-time distributions

In Figs 4 and 5, we show delay-time distributions (DTDs) for various merger channels for the triple and binary cases, respectively. We include the RLOF-induced (red lines), and tertiary unbound (dashed green lines) cases. Each panel corresponds to a different channel, labeled in the top left, and

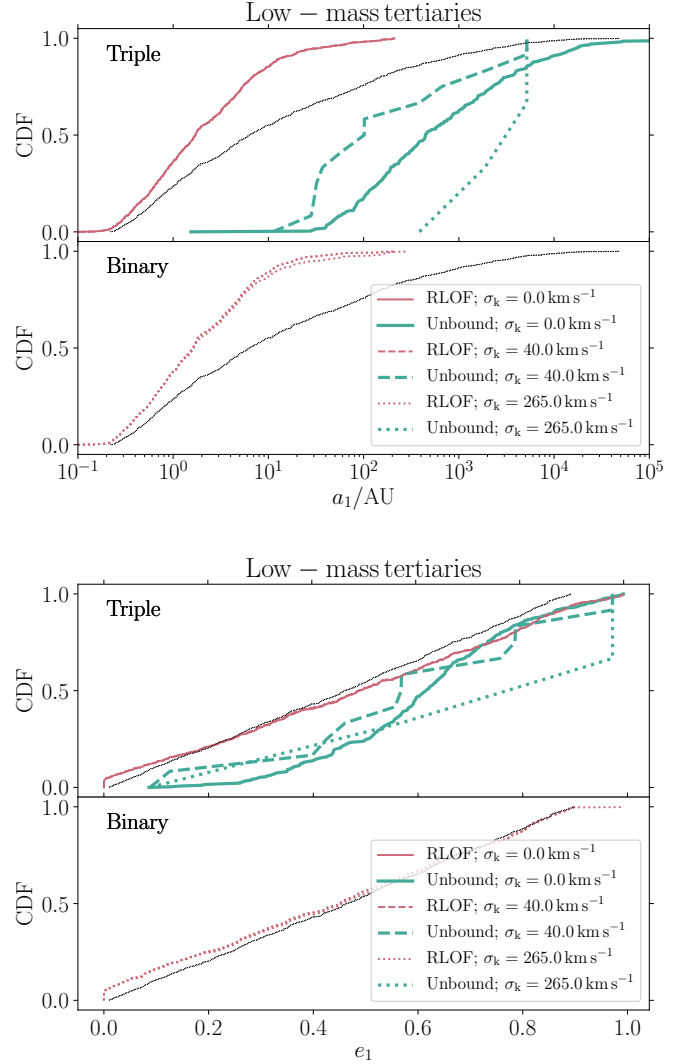


Figure 3. Similar to Fig. 2, here for the low-mass tertiary simulations. Note that the number of unbound systems in the low-mass tertiary simulations for $\sigma_k > 0 \text{ km s}^{-1}$ is very small (see the bottom row in Table 3).

we show results only for channels with a significant number of systems (≥ 5). Data apply to the simulations with $\sigma_k = 40 \text{ km s}^{-1}$, and the high-mass tertiary assumption.

Generally, RLOF-induced mergers occur earlier than tertiary unbound mergers. This can be attributed to the generally tighter orbits (see Section 4.2). There are generally no large differences between the triple (Fig. 4) and binary (Fig. 5) RLOF-induced DTDs, which can be explained by the similarities in the initial orbits.

Of most interest here are the NS-NS mergers. Most of these mergers occur within $\sim 100 \text{ Myr}$, although there is a small tail with delay times of several Gyr.

The DTDs for simulations with different parameters (low-mass tertiary, and different σ_k ; not shown here) are qualitatively similar to those in Figs 4 and 5.

4.4. Merger rates

Here, we compute the NS-NS merger rates based on the merger fractions from our simulations. To convert merger fractions to absolute rates, we start with the local star formation rate (SFR) density, which we take to be $R_{\text{SFR}} =$

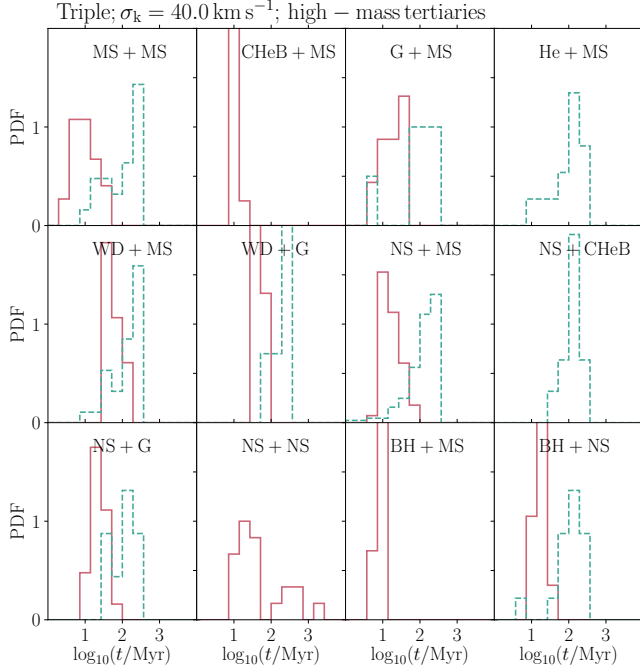


Figure 4. Delay-time distributions (DTDs) for various merger channels in the triple simulations. Refer to Fig. 5 for results from the corresponding binary case. We include the RLOF-induced (red lines), and tertiary unbound (dashed green lines) cases. Each panel corresponds to a different channel, indicated in the top left. Data apply to the simulations with $\sigma_k = 40 \text{ km s}^{-1}$, and the high-mass tertiary assumption.

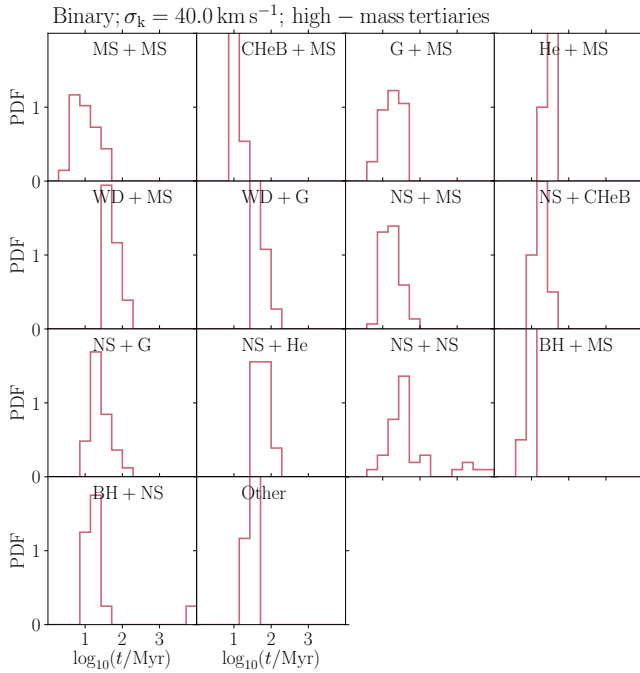


Figure 5. Similar to Fig. 4, here for the binary case. Note that the tertiary unbound case does not apply here.

$0.025 \times 10^9 \text{ M}_\odot \text{ Gpc}^{-3} \text{ yr}^{-1}$ (Bothwell et al. 2011). This is the mass of all stars formed per unit volume and time (we are agnostic about the type of galaxy in which the stars are formed and consider the local Universe only; this is justified by the typically short delay times, see Section 4.3). We assume that all stellar systems consist of either single, binary or triple stars (and ignore high-order systems). Consider a population of stars with N_{sys} stellar systems. The number of single, binary, and triple systems is then $\alpha_s N_{\text{sys}}$, $\alpha_{\text{bin}} N_{\text{sys}}$, and $\alpha_{\text{tr}} N_{\text{sys}}$, respectively, and where $\alpha_s + \alpha_{\text{bin}} + \alpha_{\text{tr}} = 1$. We assume $\alpha_s = 0.19$, $\alpha_{\text{bin}} = 0.56$, and $\alpha_{\text{tr}} = 0.25$ (Sana et al. 2014), independent of mass. We remark that other recent observational studies (e.g., Moe & Di Stefano 2017) indicate that these fractions could be more heavily biased towards more high-multiplicity systems for higher primary masses.

We assume a Kroupa (2001) initial mass function (IMF), i.e., $dN/dm \propto m^{-\alpha}$, where $\alpha = 0.3$ for $0.01 < m/\text{M}_\odot < 0.08$, $\alpha = 1.3$ for $0.08 < m/\text{M}_\odot < 0.5$, and $\alpha = 2.3$ for $m > 0.5 \text{ M}_\odot$ ³. A single-star population with N_s stars with such an IMF has a total mass of

$$M_s = \int_{m_{\text{low}}}^{m_{\text{up}}} m \frac{dN}{dm} dm = N_s \tilde{M}, \quad (4)$$

where N_s is the number of (single) stars, $m_{\text{low}} = 0.01 \text{ M}_\odot$ and $m_{\text{up}} = 150 \text{ M}_\odot$, and we calculate \tilde{M} to be $\tilde{M} \simeq 0.38 \text{ M}_\odot$ for a Kroupa (2001) IMF. In our mixed population with single, binary, and triple stars, the mass contribution from single stars is therefore $\alpha_s N_{\text{sys}} \tilde{M}$. Assuming a flat mass ratio distribution (i.e., flat in $q_1 \equiv m_2/m_1$), the binaries have a mass contribution which is approximately $(1 + \frac{1}{2}) \tilde{M} \alpha_{\text{bin}} N_{\text{sys}} = \frac{3}{2} \alpha_{\text{bin}} N_{\text{sys}} \tilde{M}$. For triples, the mass contribution depends on our assumption on the tertiary mass ratio; we assumed distributions that are flat in either $q_2 \equiv m_3/(m_1 + m_2)$, or in $q'_2 \equiv m_3/m_2$. In the former case, the mass contribution from triples is $(\frac{3}{2} + \frac{1}{2} \frac{3}{2}) \tilde{M} \alpha_{\text{tr}} N_{\text{sys}} = \frac{9}{4} \alpha_{\text{tr}} \tilde{M} N_{\text{sys}}$. In the latter case, it is $(\frac{3}{2} + \frac{1}{2} \frac{1}{2}) \tilde{M} \alpha_{\text{tr}} N_{\text{sys}} = \frac{7}{4} \alpha_{\text{tr}} \tilde{M} N_{\text{sys}}$. Adding up the contributions from all hierarchies, the total mass of our population is (in the high-mass tertiary case)

$$M_{\text{tot}} \simeq \left(\alpha_s + \frac{3}{2} \alpha_{\text{bin}} + \frac{9}{4} \alpha_{\text{tr}} \right) N_{\text{sys}} \tilde{M} = \left(1 + \frac{1}{2} \alpha_{\text{bin}} + \frac{5}{4} \alpha_{\text{tr}} \right) N_{\text{sys}} \tilde{M}. \quad (5)$$

The number of binaries/triples is therefore given by

$$N = \alpha N_{\text{sys}} = \frac{\alpha M_{\text{tot}}}{\left(1 + \frac{1}{2} \alpha_{\text{bin}} + \frac{5}{4} \alpha_{\text{tr}} \right) \tilde{M}}, \quad (6)$$

where $\alpha = \alpha_{\text{bin}}$ for binaries, and $\alpha = \alpha_{\text{tr}}$ for triples. The corresponding occurrence rates (per unit volume and time) are obtained by replacing M_{tot} in equation (6) by R_{SFR} .

To convert the total occurrence rate of binaries/triples to (NS-NS) merger rates, we need to take into account the fraction of systems that were taken into account in the simulations compared to all astrophysically-occurring systems (which we denote as f_{calc}), and the actual merger fractions in the simulations (which we denote as f_{merge}). Since we did not restrict the orbital separation distributions in the Monte Carlo simulations (see Section 3), the calculated fraction f_{calc} is determined solely by the mass cutoffs. Specifically, we restricted

³ The slope of -2.3 here is inconsistent with the assumed slope for the massive stars in our simulations (primary masses $8 < m_1/\text{M}_\odot < 50$; slope -2.35). However, the difference in slope is very small.

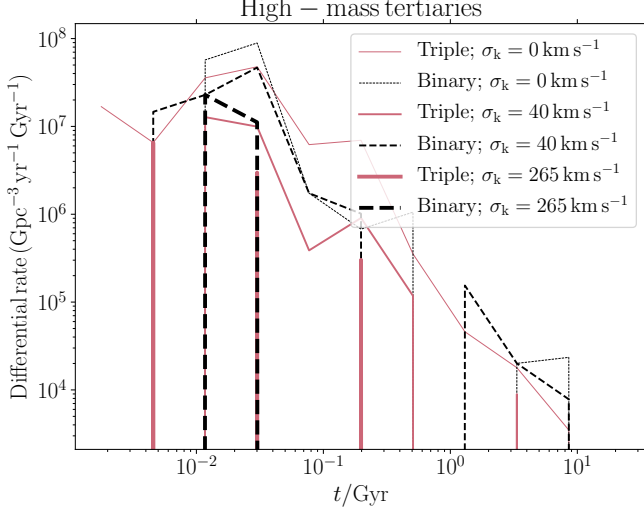


Figure 6. DTD distributions for NS-NS mergers, normalized to absolute merger rates (i.e., the integrated curves correspond to the rates given in Table 8). Red solid (black dashed) lines correspond to triples (binaries). Line thickness increases with increasing σ_k .

the primary mass to the range $8 < m_1/M_\odot < 50$ and the secondary mass to $4 < m_2/M_\odot < 50$, whereas there was no restriction on m_3 (within the mass ranges of the IMF of Kroupa 2001). For the adopted Kroupa (2001) IMF, this implies that $f_{\text{calc}} \approx 2.6 \times 10^{-3}$, which applies to both triples and binaries. The merger fractions f_{merge} can be inferred from Tables 2, 3, 4, 5, 6, and 7.

The merger rate for binaries/triples (number per unit volume and time) is then given by

$$R_{\text{merge}} \simeq \frac{\alpha R_{\text{SFR}}}{\left(1 + \frac{1}{2}\alpha_{\text{bin}} + \frac{5}{4}\alpha_{\text{tr}}\right) \tilde{M}} f_{\text{calc}} f_{\text{merge}}. \quad (7)$$

Note that this equation applies to the high-mass tertiary case; in the low-mass tertiary case, the factor $\frac{5}{4}$ in equation (7) should be replaced by $\frac{3}{4}$. The resulting NS-NS merger rates for all our simulations are given in Table 8. We also give the BH-NS merger rates in the same table. We do not include BH-BH rates, since the associated fractions f_{merge} in the simulations are at the noise level. The NS-NS DTD distributions normalized to the rates are shown in Fig. 6, and the total rates are plotted as a function of σ_k in Fig. 7. We discuss our rates further in Section 5.2.

5. DISCUSSION

5.1. The decoupling assumption

As mentioned in Section 2.2, a (strong) assumption that we made in our modeling is that, after RLOF is triggered in the inner binary system, the subsequent evolution of the inner binary is completely decoupled from the tertiary star. This approach was taken for simplicity, and current lack of the available framework to model this phase self-consistently. Here, we briefly investigate this assumption, by considering the systems that, after RLOF is triggered in the inner binary, survive the binary evolution, i.e., do not merge within 10 Gyr.

To evaluate whether or not the inner system can be decoupled from the tertiary, we compute for these systems the ratio of the timescale t_{IPN} for the lowest-order post-Newtonian (PN) precession (e.g., Weinberg 1972), to the LK timescale t_{LK} (e.g., Kinoshita & Nakai 1999; Antognini 2015). If

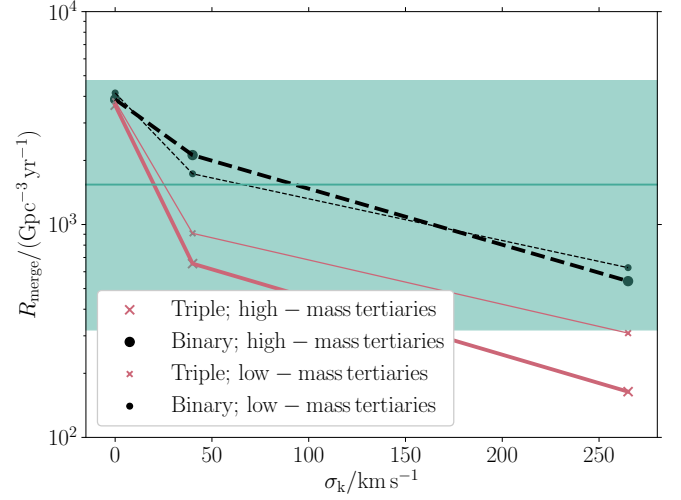


Figure 7. Total NS-NS rates plotted as a function of σ_k (the same data are quoted in Table 8). Red solid (black dashed) lines correspond to triples (binaries), and the thick (thin) lines correspond to the high (low)-mass tertiary cases. The horizontal solid green line (with green error regions) shows the LIGO rate inferred from GW170817 (Abbott et al. 2017b).

$t_{\text{IPN}} \ll t_{\text{LK}}$, we expect 1PN precession to dominate and the decoupling assumption to be justified, whereas if $t_{\text{IPN}} \gg t_{\text{LK}}$, this is no longer the case (e.g., Blaes et al. 2002; Wu & Murray 2003; Fabrycky & Tremaine 2007; Thompson 2011; Naoz et al. 2013; Liu et al. 2015).

In our simulations, we do not model the subsequent evolution of the tertiary star and orbit after the onset of RLOF. Here, we assume, for simplicity, that the tertiary mass does not change between the onset of RLOF and 10 Gyr, and make two assumptions on the outer orbit semimajor axis a_2 after 10 Gyr: we either take it to be the value at the onset of RLOF, or the value if all mass in the inner binary between the time of the onset of RLOF and 10 Gyr were lost adiabatically, i.e., with $a_2(m_1 + m_2 + m_3)$ constant.

In Fig. 8, we show the resulting distributions of the ratio $t_{\text{IPN}}/t_{\text{LK}}$, for two values of σ_k , and the high-mass tertiary simulations. As shown, there is a non-negligible fraction of systems with $t_{\text{IPN}}/t_{\text{LK}} \gg 1$, in which case the decoupling assumption is not well justified. The fraction of these systems depends on σ_k ; the distribution of $t_{\text{IPN}}/t_{\text{LK}}$ shifts to larger values with increasing σ_k .

This indicates that not all systems are well decoupled from the tertiary. This implies there is a systematic error in our results, in particular of the NS-NS merger rates. We also note that we here only considered the surviving systems; the systems undergoing RLOF may also not be truly decoupled. At this point, it is difficult to estimate whether fully self-consistent modeling would lead to lower or higher merger rates. Such an endeavor is left for future work.

5.2. Rates

Here, we comment on our NS-NS merger rates (see Section 4.4). First, as also discussed above, it should be noted that there are likely significant systematic errors in our rates as a consequence of simplifications made in the modeling. Therefore, our results should be interpreted as estimates.

Interestingly, and most importantly, the triple rates, although always lower, are typically comparable to the binary rates (see Table 8). Both the triple and binary rates are highly

	Rate ($\text{Gpc}^{-3} \text{yr}^{-1}$)					
	Triple			Binary		
	0	$\sigma_k/\text{km s}^{-1}$	0	$\sigma_k/\text{km s}^{-1}$	0	$\sigma_k/\text{km s}^{-1}$
NS-NS						
High-mass tertiary						
RLOF	1741	551	109	3874	2119	542
Unbound	1893	104	54	—	—	—
Total	3634	655	164	3874	2119	542
Low-mass tertiary						
RLOF	1937	909	309	4149	1731	627
Unbound	1856	0	0	—	—	—
Total	3793	909	309	4149	1731	627
BH-NS						
High-mass tertiary						
RLOF	166	257	268	186	840	759
Unbound	421	423	263	—	—	—
Total	586	680	531	186	840	759
Low-mass tertiary						
RLOF	109	346	345	274	747	823
Unbound	514	21	0	—	—	—
Total	622	367	345	274	747	823
NS-MS						
High-mass tertiary						
RLOF	3464	5178	7006	7710	15238	20883
Unbound	1232	4097	4650	—	—	—
Total	4697	9275	11656	7710	15238	20883
Low-mass tertiary						
RLOF	3928	7475	10351	8299	16088	23368
Unbound	1564	28	0	—	—	—
Total	5493	7504	10351	8299	16088	23368

Table 8

Compact object merger rates according to our simulations. Top part: NS-NS mergers; middle part: BH-NS mergers. We also include the rate of NS-MS mergers (Thorne-Żytkow objects) in the bottom part. We include mergers from triples and binaries, and for different kick dispersions σ_k . The assumed channels are mergers following RLOF, and after the tertiary becomes unbound from the inner binary (only applies to triples). The ‘Total’ row gives the sum of the two channels (note: quoted numbers have been rounded to integers). Results are shown for sets of simulations with the tertiary mass sampled according to $m_3 = q_2(m_1 + m_2)$ (‘high-mass tertiary’ case), and according to $m_3 = q'_2 m_2$ (‘low-mass tertiary’ case), where both q_2 and q'_2 have flat distributions.

sensitive to the SNe kick dispersion σ_k , as expected. However, the triple rates are even more sensitive to σ_k than the binary rates. This can be explained by the fact that a third star adds more possibilities for the system to become unbound, and this effect increases in importance with increasing σ_k . It should also be mentioned that we assumed a conservative triple fraction ($\alpha_{\text{tr}} = 0.25$) compared to the binary fraction ($\alpha_{\text{bin}} = 0.56$). If a higher triple fraction were assumed relative to the binary fraction, for which there is observational evidence for massive multiple systems (Moe & Di Stefano 2017), then the importance of triple systems to the NS-NS merger rate is even larger. In particular, the ratio of the triple to the binary merger rate is $\propto \alpha_{\text{tr}}/\alpha_{\text{bin}}$ (see equation 7); therefore, if we assumed, e.g., $\alpha_{\text{tr}} = 0.5$ and $\alpha_{\text{bin}} = 0.4$ instead of $\alpha_{\text{tr}} = 0.25$ and $\alpha_{\text{bin}} = 0.56$, this ratio would increase by a factor of ≈ 3 .

Our rates vary from typically several hundred to several thousand $\text{Gpc}^{-3} \text{yr}^{-1}$, strongly depending on σ_k . The rate inferred by GW170817 is $1540^{+3200}_{-1220} \text{Gpc}^{-3} \text{yr}^{-1}$ (Abbott et al. 2017b), which falls well within our ranges (for both triples and binaries). Based on observations of short gamma-ray bursts, Coward et al. (2012) find

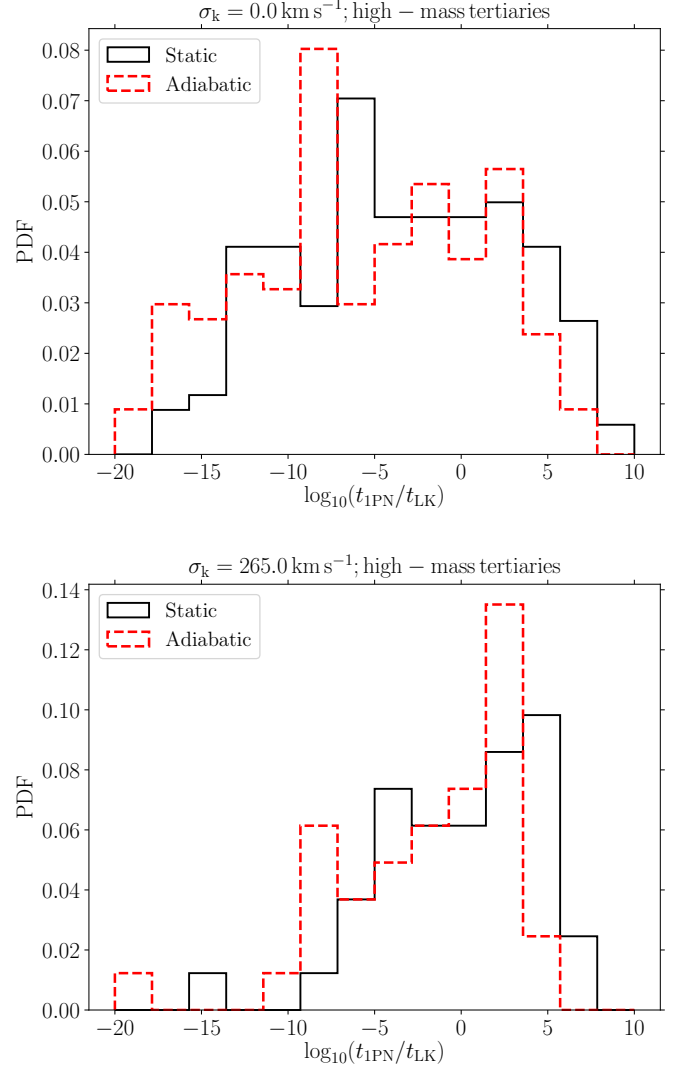


Figure 8. Distributions of the ratio $t_{\text{1PN}}/t_{\text{LK}}$ for systems in which RLOF was triggered in the inner binary, but which do not merge within 10 Gyr according to BSE. The top (bottom) panels assume $\sigma_k = 0 \text{ km s}^{-1}$ ($\sigma_k = 265 \text{ km s}^{-1}$), and data are taken from the high-mass tertiary simulations (the distributions are similar for the low-mass tertiary simulations). Two assumptions are made on the outer orbit semimajor axis a_2 after 10 Gyr: we either take it to be the value at the onset of RLOF (‘static’; black solid lines), or the value if all mass in the inner binary between the time of the onset of RLOF and 10 Gyr were lost adiabatically, i.e., with $a_2(m_1 + m_2 + m_3)$ constant (‘adiabatic’; red dashed lines).

a rate of $\sim 8 - 1800 \text{Gpc}^{-3} \text{yr}^{-1}$, Petrillo et al. (2013) of $\sim 500 - 1500 \text{Gpc}^{-3} \text{yr}^{-1}$, Siellez et al. (2014) of $\sim 92 - 1154 \text{Gpc}^{-3} \text{yr}^{-1}$, and Fong et al. (2015) of $\sim 90 - 1850 \text{Gpc}^{-3} \text{yr}^{-1}$, also consistent with our rates.

Theoretical studies based on isolated binary evolution typically find NS-NS merger rates of several tens to hundreds $\text{Gpc}^{-3} \text{yr}^{-1}$, up to order thousand in extreme cases. For example, Belczynski et al. (2016b) found rates of $\sim 50 - 150 \text{Gpc}^{-3} \text{yr}^{-1}$, and Kruckow et al. (2018) found rates of $\sim 10 - 400 \text{Gpc}^{-3} \text{yr}^{-1}$ (the upper limit being ‘rather optimistic’). The rates are highly sensitive to the CE α parameter, as shown by Giacobbo & Mapelli (2018), who found rates up to several hundred $\text{Gpc}^{-3} \text{yr}^{-1}$ and up to $\sim 10^3 \text{Gpc}^{-3} \text{yr}^{-1}$ if a high CE α value is assumed, and Chruslinska et al. (2018), who found similar results. Another crucial ingredient is the

assumption on natal kicks (e.g., [Giacobbo & Mapelli 2019](#)).

Generally, isolated binary evolution studies find rates that are lower than our ‘binary’ rates, as listed in Table 8. This can be understood by noting that our ‘binary’ population consists of the inner binaries of a triple population. The requirement of dynamical stability implies that the inner binary separation distribution becomes skewed towards smaller values. As can be seen in Fig. 2 (see the black dotted lines), the inner binary semimajor axis distribution of the binaries in our simulations has a median value of ≈ 10 AU. In contrast, for a distribution flat in $\log_{10}(a_1)$ without the restriction of dynamical stability imposed by the tertiary, the median semimajor axis is $a_{\text{low}}(a_{\text{up}}/a_{\text{low}})^{1/2} \approx 32$ AU (setting $a_{\text{low}} = 0.02$ AU, and $a_{\text{up}} = 5 \times 10^4$ AU, see Fig. 2). A more compact distribution of semimajor axes implies a higher formation rate of double NS binaries, explaining the higher base binary NS-NS merger rate in our simulations. Another way of understanding this trend is by noting that a more compact initial semimajor axis distribution is somewhat analogous to assuming a higher CE efficiency. The latter indeed leads to higher merger rates, of several hundred and up to $\sim 10^3$ $\text{Gpc}^{-3} \text{yr}^{-1}$ ([Giacobbo & Mapelli 2018](#)).

6. CONCLUSIONS

In this paper, we estimated the rates of mergers of double neutron stars (NSs) in triple systems. We took into account secular, stellar, tidal and binary evolution, and the effects of supernovae (SNe) on the orbits, starting with main-sequence (MS) stars, until the merger of two NSs. We made different assumptions on the properties of the massive triple progenitors, including different kick distributions, and different assumptions on the tertiary mass distribution. Our main conclusions are given below.

1. Contrary to previous studies of the secular and stellar evolution of triples which focused on wide inner binaries that do not interact in the absence of a tertiary star (e.g., [Hamers et al. 2013](#); [Antonini et al. 2017](#); [Hamers & Thompson 2019](#)), we found that the tertiary does not significantly affect the probability of Roche-lobe overflow (RLOF) in the inner binary system. This can be attributed to the fact that we did not restrict to wide, non-interacting systems, but instead considered the entire range of orbital separations. Consequently, the inner binary interacts also in the absence of the tertiary star. Typically, about 60% of systems undergo RLOF in our simulations, for both triple and binary cases (in the latter case, the same inner binary parameters are adopted, but without taking into account the effects of the tertiary star). We modeled the subsequent evolution of RLOF systems using a binary population synthesis code, neglecting the effect of the tertiary. Subsequently, the stars in the inner binary can merge as two NSs after periods of mass transfer and/or common-envelope evolution. Future work should not make the simplifying decoupling assumption, but model the system self-consistently (see Section 5.1).

2. For ~ 10 up to $\sim 50\%$ of systems, the inner and/or outer binary becomes unbound due to the effects of SNe (instantaneous mass loss and/or the effects of SNe kicks). Kicks are typically more important for triples, since a third star adds more possibilities for the system to become unbound, and this effect increases in importance with increasing kick dispersion. In up to $\sim 30\%$ of simulated triples, the inner binary remains bound after a SNe event whereas the tertiary star becomes

unbound. The inner binaries of these systems can still potentially merge at a later time due to ‘isolated binary’ evolution. We continued the evolution of these isolated binaries using a binary population synthesis code (and considered these systems to be part of the original ‘triple’ population). The fraction of triple systems without strong interactions is small, typically a few per cent. This can be attributed to the large RLOF fraction (due to the inclusion of tighter systems), and the importance of SNe kicks, especially for NSs.

3. We considered two pathways for NS-NS mergers in triples: following binary interactions after RLOF (possibly induced by the tertiary star through Lidov-Kozai oscillations), or following binary interactions after the inner binary became unbound from the tertiary due to a SNe event. For the equivalent binaries (with the same properties as the inner binaries of the triples that we modeled), we considered only the channel of mergers following binary interactions after RLOF. Our rates (see Fig. 7 for a visual summary) vary from typically several hundred to several thousand $\text{Gpc}^{-3} \text{yr}^{-1}$, and are within the rate estimates of LIGO based on GW170817, $1540^{+3200}_{-1220} \text{Gpc}^{-3} \text{yr}^{-1}$ ([Abbott et al. 2017b](#)). We find that the rates decrease strongly with increasing SNe kick speed, σ_k . Also, the ratio of the triple to binary NS-NS merger rate decreases with increasing σ_k . Our ‘binary’ rates are higher compared to dedicated isolated binary evolution studies. This can be understood from the more compact inner binaries in our simulations, which are the result of the requirement of dynamical stability of the corresponding triple system.

4. Most of the NS-NS mergers in our models occur relatively early, with a delay-time distribution (DTD) peaked around several tens of Myr. Some mergers can occur at late times, of several Gyr.

5. We also considered mergers of other types of stars (see Figs. 4 and 5). In particular, we found a large fraction of NS-MS mergers in both triple and binary cases. Such mergers result in Thorne-Żytkow objects ([Thorne & Zytkov 1977](#)), and are also found in dedicated isolated binary evolution studies (e.g., [Brandt & Podsiadlowski 1995](#)). Our results show that this channel is also possible (and relatively likely) in triples; in fact, the fractions of Thorne-Żytkow objects in our simulations are very similar in the triple and binary cases, giving formation rates on the order of several thousand $\text{Gpc}^{-3} \text{yr}^{-1}$ (see Table 8). Taking into account the occurrence rates of triples and binaries, the relative formation rate of these objects formed in our simulations ranges between $R_{\text{TZ,triple}}/R_{\text{TZ,binary}} \sim 0.4$ to ~ 0.6 (depending on the assumed kick speed and tertiary mass ratio distributions). In addition, we found BH-NS mergers at a rate of typically several hundred $\text{Gpc}^{-3} \text{yr}^{-1}$ (see Table 8).

ACKNOWLEDGEMENTS

We thank the anonymous referee for a helpful report. A.S.H. gratefully acknowledges support from the Institute for Advanced Study, and the Martin A. and Helen Chooljian Membership. T.A.T. is supported in part by a Simons Foundation Fellowship, an IBM Einstein Fellowship from the Institute for Advanced Study, NSF grant 1313252, and Scialog Scholar grant 24216 from the Research Corporation.

REFERENCES

Abadie, J., Abbott, B. P., Abbott, R., et al. 2010, *Classical and Quantum Gravity*, 27, 173001

- Abbott, B. P., Abbott, R., Abbott, T. D., et al. 2017a, *ApJ*, **848**, L13
- . 2017b, *Phys. Rev. Lett.*, **119**, 161101
- Alexander, K. D., Berger, E., Fong, W., et al. 2017, *ApJ*, **848**, L21
- Antognini, J. M., Shappee, B. J., Thompson, T. A., & Amaro-Seoane, P. 2014, *MNRAS*, **439**, 1079
- Antognini, J. M. O. 2015, *MNRAS*, **452**, 3610
- Antonini, F., Murray, N., & Mikkola, S. 2014, *ApJ*, **781**, 45
- Antonini, F., & Perets, H. B. 2012, *ApJ*, **757**, 27
- Antonini, F., & Rasio, F. A. 2016, *ApJ*, **831**, 187
- Antonini, F., Toonen, S., & Hamers, A. S. 2017, *ApJ*, **841**, 77
- Arca-Sedda, M., & Capuzzo-Dolcetta, R. 2019, *MNRAS*, **483**, 152
- Arca-Sedda, M., & Gualandris, A. 2018, *MNRAS*, **477**, 4423
- Arzoumanian, Z., Chernoff, D. F., & Cordes, J. M. 2002, *ApJ*, **568**, 289
- Barker, A. J., & Ogilvie, G. I. 2009, *MNRAS*, **395**, 2268
- Belczynski, K., Buonanno, A., Cantiello, M., et al. 2014, *ApJ*, **789**, 120
- Belczynski, K., Holz, D. E., Bulik, T., & O’Shaughnessy, R. 2016a, *Nature*, **534**, 512
- Belczynski, K., Kalogera, V., & Bulik, T. 2002, *ApJ*, **572**, 407
- Belczynski, K., Repetto, S., Holz, D. E., et al. 2016b, *ApJ*, **819**, 108
- Belczynski, K., Klencki, J., Meynet, G., et al. 2017, ArXiv e-prints, [arXiv:1706.07053](https://arxiv.org/abs/1706.07053) [astro-ph.HE]
- Beniamini, P., & Piran, T. 2016, *MNRAS*, **456**, 4089
- Berger, E. 2014, *ARA&A*, **52**, 43
- Blaauw, A. 1961, Bulletin of the Astronomical Institutes of the Netherlands, **15**, 265
- Blaes, O., Lee, M. H., & Socrates, A. 2002, *ApJ*, **578**, 775
- Bode, J. N., & Wegg, C. 2014, *MNRAS*, **438**, 573
- Boersma, J. 1961, Bull. Astron. Inst. Netherlands, **15**, 291
- Bonetti, M., Perego, A., Capelo, P. R., Dotti, M., & Miller, M. C. 2018, *PASA*, **35**, e017
- Bothwell, M. S., Kennicutt, R. C., Johnson, B. D., et al. 2011, *MNRAS*, **415**, 1815
- Brandt, N., & Podsiadlowski, P. 1995, *MNRAS*, **274**, 461
- Chornock, R., Berger, E., Kasen, D., et al. 2017, *ApJ*, **848**, L19
- Chruslinska, M., Belczynski, K., Klencki, J., & Benacquista, M. 2018, *MNRAS*, **474**, 2937
- Coulter, D. A., Foley, R. J., Kilpatrick, C. D., et al. 2017, *Science*, **358**, 1556
- Coward, D. M., Howell, E. J., Piran, T., et al. 2012, *MNRAS*, **425**, 2668
- Cowperthwaite, P. S., Berger, E., Villar, V. A., et al. 2017, *ApJ*, **848**, L17
- Čuk, M., & Burns, J. A. 2004, *AJ*, **128**, 2518
- Dominik, M., Belczynski, K., Fryer, C., et al. 2012, *ApJ*, **759**, 52
- . 2013, *ApJ*, **779**, 72
- Duchêne, G., & Kraus, A. 2013, *ARA&A*, **51**, 269
- Eggleton, P. P., Kiseleva, L. G., & Hut, P. 1998, *ApJ*, **499**, 853
- Eggleton, P. P., & Kiseleva-Eggleton, L. 2001, *ApJ*, **562**, 1012
- Eichler, D., Livio, M., Piran, T., & Schramm, D. N. 1989, *Nature*, **340**, 126
- Fabrycky, D., & Tremaine, S. 2007, *ApJ*, **669**, 1298
- Fong, W., Berger, E., Margutti, R., & Zauderer, B. A. 2015, *ApJ*, **815**, 102
- Fragione, G., Grishin, E., Leigh, N. W. C., Perets, H. B., & Perna, R. 2018, ArXiv e-prints, [arXiv:1811.10627](https://arxiv.org/abs/1811.10627)
- Fragione, G., & Loeb, A. 2019, *MNRAS*, **486**, 4443
- Freiburghaus, C., Rosswog, S., & Thielemann, F. K. 1999, *ApJ*, **525**, L121
- Fryer, C. L., Belczynski, K., Wiktorowicz, G., et al. 2012, *ApJ*, **749**, 91
- Giacobbo, N., & Mapelli, M. 2018, *MNRAS*, **480**, 2011
- . 2019, *MNRAS*, **482**, 2234
- Goldstein, A., Veres, P., Burns, E., et al. 2017, *ApJ*, **848**, L14
- Gondán, L., Kocsis, B., Raffai, P., & Frei, Z. 2018, *ApJ*, **860**, 5
- Grishin, E., Perets, H. B., & Fragione, G. 2018, *MNRAS*, **481**, 4907
- Hamers, A. S. 2018a, *MNRAS*, **478**, 620
- . 2018b, *MNRAS*, **476**, 4139
- Hamers, A. S., Bar-Or, B., Petrovich, C., & Antonini, F. 2018, *ApJ*, **865**, 2
- Hamers, A. S., & Dosopoulou, F. 2019, *ApJ*, **872**, 119
- Hamers, A. S., Pols, O. R., Claeys, J. S. W., & Nelemans, G. 2013, *MNRAS*, **430**, 2262
- Hamers, A. S., & Portegies Zwart, S. F. 2016a, *MNRAS*, **459**, 2827
- . 2016b, *MNRAS*, **462**, L84
- Hamers, A. S., & Thompson, T. A. 2019, ArXiv e-prints, [arXiv:1904.12881](https://arxiv.org/abs/1904.12881)
- Hansen, B. M. S., & Phinney, E. S. 1997, *MNRAS*, **291**, 569
- Hoang, B.-M., Naoz, S., Kocsis, B., Rasio, F. A., & Dosopoulou, F. 2018, *ApJ*, **856**, 140
- Hobbs, G., Lorimer, D. R., Lyne, A. G., & Kramer, M. 2005, *MNRAS*, **360**, 974
- Huang, S. S. 1956, *AJ*, **61**, 49
- Huang, S.-S. 1963, *ApJ*, **138**, 471
- Hurley, J. R., Pols, O. R., & Tout, C. A. 2000, *MNRAS*, **315**, 543
- Hurley, J. R., Tout, C. A., & Pols, O. R. 2002, *MNRAS*, **329**, 897
- Hut, P. 1981, *A&A*, **99**, 126
- Ivanov, P. B., Polnarev, A. G., & Saha, P. 2005, *MNRAS*, **358**, 1361
- Just, O., Bauswein, A., Ardevol Pulpillo, R., Goriely, S., & Janka, H. T. 2015, *MNRAS*, **448**, 541
- Kaib, N. A., & Raymond, S. N. 2014, *ApJ*, **782**, 60
- Kalogera, V., Belczynski, K., Kim, C., O’Shaughnessy, R., & Willems, B. 2007, *Phys. Rep.*, **442**, 75
- Kalogera, V., Kim, C., Lorimer, D. R., et al. 2004a, *ApJL*, **614**, L137
- . 2004b, *ApJL*, **601**, L179
- Katz, B., & Dong, S. 2012, ArXiv e-prints, [arXiv:1211.4584](https://arxiv.org/abs/1211.4584) [astro-ph.SR]
- Kimpson, T. O., Spera, M., Mapelli, M., & Ziosi, B. M. 2016, *MNRAS*, **463**, 2443
- Kinoshita, H., & Nakai, H. 1999, *Celestial Mechanics and Dynamical Astronomy*, **75**, 125
- Kobulnicky, H. A., Kiminki, D. C., Lundquist, M. J., et al. 2014, *ApJS*, **213**, 34
- Kozai, Y. 1962, *AJ*, **67**, 591
- Kroupa, P. 2001, *MNRAS*, **322**, 231
- Kruckow, M. U., Tauris, T. M., Langer, N., Kramer, M., & Izzard, R. G. 2018, *MNRAS*, **481**, 1908
- Lattimer, J. M., & Schramm, D. N. 1974, *ApJ*, **192**, L145
- Lei, H., Circi, C., & Ortore, E. 2018, *MNRAS*, **481**, 4602
- Lidov, M. L. 1962, *Planet. Space Sci.*, **9**, 719
- Lipunov, V. M., Postnov, K. A., & Prokhorov, M. E. 1997, *Astronomy Letters*, **23**, 492
- Liu, B., & Lai, D. 2017, *ApJL*, **846**, L11
- . 2018, *ApJ*, **863**, 68
- Liu, B., Lai, D., & Wang, Y.-H. 2019, ArXiv e-prints, [arXiv:1905.00427](https://arxiv.org/abs/1905.00427)
- Liu, B., Muñoz, D. J., & Lai, D. 2015, *MNRAS*, **447**, 747
- Lu, C. X., & Naoz, S. 2019, *MNRAS*, **484**, 1506
- Luo, L., Katz, B., & Dong, S. 2016, *MNRAS*, **458**, 3060
- Mapelli, M. 2016, *MNRAS*, **459**, 3432
- Mardling, R. A., & Aarseth, S. J. 2001, *MNRAS*, **321**, 398
- Margutti, R., Berger, E., Fong, W., et al. 2017, *ApJ*, **848**, L20
- Metzger, B. D., Martínez-Pinedo, G., Darbha, S., et al. 2010, *MNRAS*, **406**, 2650
- Michael, E., & Perets, H. B. 2019, ArXiv e-prints, [arXiv:1902.01864](https://arxiv.org/abs/1902.01864)
- Miller, M. C., & Hamilton, D. P. 2002, *ApJ*, **576**, 894
- Moe, M., & Di Stefano, R. 2017, *ApJS*, **230**, 15
- Naoz, S. 2016, *ARA&A*, **54**, 441
- Naoz, S., Fragos, T., Geller, A., Stephan, A. P., & Rasio, F. A. 2016, *ApJL*, **822**, L24
- Naoz, S., Kocsis, B., Loeb, A., & Yunes, N. 2013, *ApJ*, **773**, 187
- Nicholl, M., Berger, E., Kasen, D., et al. 2017, *ApJ*, **848**, L18
- Ogilvie, G. I. 2014, *ARA&A*, **52**, 171
- O’Leary, R. M., Rasio, F. A., Fregeau, J. M., Ivanova, N., & O’Shaughnessy, R. 2006, *ApJ*, **637**, 937
- Öpik, E. 1924, Publications of the Tartu Astrofizika Observatory, **25**
- Pelupessy, F. I., van Elteren, A., de Vries, N., et al. 2013, *A&A*, **557**, A84
- Perets, H. B., & Kratter, K. M. 2012, *ApJ*, **760**, 99
- Petrillo, C. E., Dietz, A., & Cavaglià, M. 2013, *ApJ*, **767**, 140
- Petrovich, C., & Antonini, F. 2017, *ApJ*, **846**, 146
- Pian, E., D’Avanzo, P., Benetti, S., et al. 2017, *Nature*, **551**, 67
- Piran, T. 1999, *Phys. Rep.*, **314**, 575
- Portegies Zwart, S., McMillan, S. L. W., van Elteren, E., Pelupessy, I., & de Vries, N. 2013, *Computer Physics Communications*, **183**, 456
- Portegies Zwart, S. F., & McMillan, S. L. W. 2000, *ApJL*, **528**, L17
- Prodan, S., Antonini, F., & Perets, H. B. 2015, *ApJ*, **799**, 118
- Randall, L., & Xianyu, Z.-Z. 2018a, *ApJ*, **864**, 134
- . 2018b, *ApJ*, **853**, 93
- Rodríguez, C. L., Amaro-Seoane, P., Chatterjee, S., & Rasio, F. A. 2018, *Physical Review Letters*, **120**, 151101
- Rodríguez, C. L., Chatterjee, S., & Rasio, F. A. 2016, *Phys. Rev. D*, **93**, 084029
- Rodríguez, C. L., Morscher, M., Pattabiraman, B., et al. 2015, *Physical Review Letters*, **115**, 051101
- Rose, S. C., Naoz, S., & Geller, A. M. 2019, *MNRAS*, **488**, 2480
- Rosswog, S. 2015, *International Journal of Modern Physics D*, **24**, 1530012
- Salpeter, E. E. 1955, *ApJ*, **121**, 161
- Samsing, J. 2018, *Phys. Rev. D*, **97**, 103014
- Samsing, J., Askar, A., & Giersz, M. 2018a, *ApJ*, **855**, 124
- Samsing, J., MacLeod, M., & Ramirez-Ruiz, E. 2018b, *ApJ*, **853**, 140
- Samsing, J., & Ramirez-Ruiz, E. 2017, *ApJL*, **840**, L14
- Sana, H., de Mink, S. E., de Koter, A., et al. 2012, *Science*, **337**, 444
- Sana, H., Le Bouquin, J. B., Lacour, S., et al. 2014, *ApJS*, **215**, 15
- Savchenko, V., Ferrigno, C., Kuulkers, E., et al. 2017, *ApJ*, **848**, L15
- Sepinsky, J. F., Willems, B., & Kalogera, V. 2007, *ApJ*, **660**, 1624

- Seto, N. 2013, [Physical Review Letters](#), **111**, 061106
- Shappee, B. J., & Thompson, T. A. 2013, [ApJ](#), **766**, 64
- Shappee, B. J., Simon, J. D., Drout, M. R., et al. 2017, [Science](#), **358**, 1574
- Siellez, K., Boër, M., & Gendre, B. 2014, [MNRAS](#), **437**, 649
- Sigurdsson, S., & Hernquist, L. 1993, [Nature](#), **364**, 423
- Silsbee, K., & Tremaine, S. 2017, [ApJ](#), **836**, 39
- Soares-Santos, M., Holz, D. E., Annis, J., et al. 2017, [ApJ](#), **848**, L16
- Stephan, A. P., Naoz, S., Ghez, A. M., et al. 2016, [MNRAS](#), **460**, 3494
- . 2019, [ApJ](#), **878**, 58
- Stevenson, S., Vigna-Gómez, A., Mandel, I., et al. 2017, [Nature Communications](#), **8**, 14906
- Thompson, T. A. 2011, [ApJ](#), **741**, 82
- Thorne, K. S., & Zytlow, A. N. 1977, [ApJ](#), **212**, 832
- Tokovinin, A. 2017, [ApJ](#), **844**, 103
- Toonen, S., Perets, H. B., & Hamers, A. S. 2018, [A&A](#), **610**, A22
- Tutukov, A., & Yungelson, L. 1973, [Nauchnye Informatsii](#), **27**, 70
- Tutukov, A. V., & Yungelson, L. R. 1993, [MNRAS](#), **260**, 675
- Tutukov, A. V., Yungelson, L. R., & Iben, Icko, J. 1992, [ApJ](#), **386**, 197
- VanLandingham, J. H., Miller, M. C., Hamilton, D. P., & Richardson, D. C. 2016, [ApJ](#), **828**, 77
- Voss, R., & Tauris, T. M. 2003, [MNRAS](#), **342**, 1169
- Weinberg, S. 1972, [Gravitation and Cosmology: Principles and Applications of the General Theory of Relativity](#), 688
- Wen, L. 2003, [ApJ](#), **598**, 419
- Wu, Y., & Murray, N. 2003, [ApJ](#), **589**, 605
- Ziosi, B. M., Mapelli, M., Branchesi, M., & Tormen, G. 2014, [MNRAS](#), **441**, 3703